HHS Public Access

Author manuscript

Nat Cell Biol. Author manuscript; available in PMC 2023 August 01.

Published in final edited form as:

Nat Cell Biol. 2023 February ; 25(2): 222–234. doi:10.1038/s41556-022-01065-w.

Progenitor-derived endothelin controls dermal sheath contraction for hair follicle regression

Pieter Martino[#,1,2], **Raghava Sunkara**[#,1,2], **Nicholas Heitman**[1,2,3], **Martina Rangl**[1,2], **Alexia Brown**[1,2], **Nivedita Saxena**[1,2,3], **Laura Grisanti**[1,2], **Donald Kohan**[5], **Masashi Yanagisawa**[6], **Michael Rendl**[1,2,3,4,*]

[1]Black Family Stem Cell Institute, Icahn School of Medicine at Mount Sinai, Atran Building AB7-10C, Box 1020; 1428 Madison Ave, New York, NY 10029, USA

[2]Department of Cell, Developmental and Regenerative Biology, Icahn School of Medicine at Mount Sinai, Atran Building AB7-10C, Box 1020; 1428 Madison Ave, New York, NY 10029, USA

[3]Graduate School of Biomedical Sciences, Icahn School of Medicine at Mount Sinai, Atran Building AB7-10C, Box 1020; 1428 Madison Ave, New York, NY 10029, USA

[4]Department of Dermatology; Icahn School of Medicine at Mount Sinai, Atran Building AB7-10C, Box 1020; 1428 Madison Ave, New York, NY 10029, USA

[5]Division of Nephrology, University of Utah Health, Salt Lake City, UT 84132, USA

[6]International Institute for Integrative Sleep Medicine, University of Tsukuba, Tsukuba, Japan

Abstract

Drastic follicle remodeling during the regression phase of the hair growth cycle is coordinated by contraction of the dermal sheath (DS) smooth muscle, but how DS-generated forces are regulated is unknown. Here, we identify spatiotemporally controlled endothelin signaling – a potent vasoconstriction-regulating pathway – as the key activating mechanism of DS contraction. Pharmacological blocking or genetic ablation of both endothelin receptors, ET_A and ET_B, impedes DS contraction and halts follicle regression. Epithelial progenitors at the club hair/strand bottleneck produce the endothelin ligand ET-1 required for follicle regression. ET signaling in DS cells and downstream contraction is dynamically regulated by cytoplasmic Ca^{2+} levels via cell membrane and sarcoplasmic reticulum calcium channels. Together, these findings illuminate an epithelial-mesenchymal-interaction paradigm in which progenitors – destined to undergo programmed cell death – control the contraction of the surrounding sheath smooth muscle to orchestrate homeostatic tissue regression and reorganization for the next stem cell activation and regeneration cycle.

[*]Author for correspondence (michael.rendl@mssm.edu).
[#]Contributed equally

AUTHOR CONTRIBUTIONS

P.M., R.S., N.H., and M.R. designed the experiments and overall study. P.M. and M.R. wrote the manuscript. P.M., R.S., N.H., A.B., N.S., and L.G. performed the experiments. D.K. and M.Y. assisted with data analysis and manuscript writing. M.R. supervised the study.

COMPETING INTERESTS

The authors declare no competing interests.

Keywords

Dermal sheath; Endothelin; Cellular contraction; Stem cell niche; Dermal papilla; Hair follicle cycling

INTRODUCTION

Adult stem cells and progenitors rely on dynamic interactions with the microenvironment, or niche, to execute their organ-specific functions including replenishing lost cells during homeostatic tissue turnover or following injury[1–3]. Cell-cell communication among heterologous cell types within the niche via paracrine signaling is a central mechanism regulating stem cell behavior[4–7]. In recent years, physical and mechanical niche inputs have been increasingly recognized as stem cell-regulating niche factors[8–10].

Strategies to offset cell addition with loss differ across stem cell pools depending on the dynamics of homeostatic turnover and regeneration[11,12]. In the hair follicle (HF) growth cycle, periodic regeneration of resting-phase HFs depends upon transient expansion of epithelial stem cells in the bulge and germ region[13–16], activated by signals from the neighboring dermal papilla (DP), a cluster of specialized mesenchymal cells[4,5,17]. The stem cells during follicle downgrowth give rise to progenitor populations of the outer root sheath (ORS) and matrix compartment of the fully regenerated HF[18,19]. The progenitors at the HF base then fuel hair shaft production during hair growth, which is coordinated by niche signals from the DP[20–22] that itself also relocates to the HF base. After the growth phase, follicle regression ensues with coordinated progenitor apoptosis and HF involution[23,24], followed by a resting phase before the hair growth cycle begins anew with stem cell activation by the DP[17,25–27].

A preponderance of stem cell niche studies in the HF have focused on the regulation of the rest-to-growth transition of the hair growth cycle illuminating key roles of the niche in controlling follicle regeneration[26,27]. Mechanisms that regulate regression – which counterbalances tissue growth to maintain homeostasis – are less well understood. During regression, rapid cessation of progenitor proliferation and differentiation is followed by apoptosis and massive reduction of the cell pool along the entire follicle length[23,24] with only a small subset of ORS progenitors persisting that give rise to the bulge and germ stem cells of the fully regressed, resting-phase follicle[18,28]. Besides progenitor pruning, the involution-like regression of over 80% of the follicle length involves hair shaft extrusion and long-distance relocation of the DP from the proximal follicle base to the stem cells at the distal tip[29]. This drastic follicle remodeling is accomplished by mechanical forces generated by the dermal sheath (DS) smooth muscle[29,30]. The DS contracts at the ‘club hair-epithelial strand’ interface to push the shaft upward and move the DP to the stem cell reservoir-adjacent position by the resting phase[29].

Several signaling pathways have been identified that regulate the growth-to-regression transition and control progenitor death during regression[23,24,31]. However, which molecular signals regulate DS contraction and follicle regression remained unknown. Here, we identify with transcriptomic analyses coupled with functional pharmacological and genetic

experiments a critical role for spatiotemporally controlled endothelin signaling crosstalk between the HF epithelium and mesenchyme in regulating DS contraction and thus the entire regression phase of the hair cycle. Overall, our results uncover a signaling mechanism by which smooth muscle contraction in a stem cell niche counterbalances growth with regression to maintain tissue homeostasis.

RESULTS

The DS smooth muscle expresses both endothelin receptors

Smooth muscle contraction of the DS is essential for the regression movements that remodel the HF stem cell niche for subsequent stem cell activation and regeneration in the hair growth cycle[29]. To uncover the regulatory controls of DS contraction (Fig. 1a), we freshly isolated DS cells from early-onset regressing follicles and systematically analyzed their transcriptome for expression of signaling pathways known to regulate smooth muscle contraction[32].

We first obtained pure DS by fluorescence activated cell sorting of digested back skins from postnatal (P) day 16 triple-fluorescent *Tbx18^{H2BGFP};Crabp1-GFP;Lef1-RFP* reporter mice (Fig. 1b)[33–35]. At P16, most HFs have entered early regression with shutdown of cell proliferation (pH3) and onset of apoptosis (Casp3^{+}) in the thinning hair bulb (Extended Data Fig. 1a). *Tbx18^{H2BGFP}* is highly expressed in the DS (Fig. 1b and Extended Data Fig. 1b,c) and at lower levels in the lineage-related DP[35]. *Crabp1-GFP* is expressed only in the DP (Extended Data Fig. 1d) and *Lef1-RFP* marks the DP as well as dermal fibroblasts (DF)[35]. Together with immunofluorescence for DS/arrector pili muscle marker ITGA8 and pan-mesenchymal marker PDGFRA (Fig. 1c; Extended Data Fig. 1b–d), the labeling combinations facilitated the simultaneous isolation of enriched DS, DP and DF (Fig. 1c).

We then performed mRNA sequencing on lysates from each of these bulk isolated populations and ran the whole-transcriptome data through established transcriptomics analyses pipelines[36]. Principal component analysis (Extended Data Fig. 2a) and hierarchical clustering (Fig. 1d) determined the unique gene-expression patterns of each population reflecting their specialized functions. Comparative gene expression analysis established molecular signatures of DS cells, DP and DF at regression onset (Fig. 1e; Supplementary Table 1), showing enrichment of cell-type specific genes (Extended Data Fig. 2b). The DS signature genes were enriched for multiple functional gene categories including actomyosin structure organization, vascular associated smooth muscle contraction, and regulation of cell communication (Extended Data Fig. 2c,d). Of all categories, most significantly enriched was “muscle contraction”, in which endothelin receptor A and B genes, *Ednra* and *Ednrb*, stood out (Fig. 1f) since endothelin signaling is a well-known pathway that regulates vascular smooth muscle contraction for vasoconstriction[37,38] and thus could be a key regulator of DS contraction during hair regression.

We next determined the *Ednra* and *Ednrb* expression levels and surveyed their relative abundance in comparison to all the known receptors of signaling pathways that control vasoconstriction of blood vessel smooth muscle cells or that operate to regulate contraction of other smooth muscles[32,39] (Fig. 1g). Among the muscarinic acetylcholine (*Chrm*)

and alpha-1 adrenergic (*Adra*) receptors, angiotensin (*Agtr*) and endothelin receptors (*Ednr*), as well as arginine vasopressin (*Avpr*), neuropeptide Y (*Npyr*), purinergic (*P2rx*), 5-hydroxytryptamine (*5-HT*), urotensin II (*Uts2r*), kisspeptin (*Kiss*) and thromboxane receptors (*Tbxa2r*), the DS expressed remarkably high levels only of the two endothelin receptor transcripts. This suggests that endothelin signaling may be the main contraction-activating pathway that operates in DS cells.

To determine how selective endothelin receptor genes *Ednra* and *Ednrb* are expressed in the DS, we compared their expression levels to those of DP and DF. Expression of both endothelin receptor transcripts is highly enriched in DS cells consistent with selective contraction activation in these specialized smooth muscle cells (Fig. 1h). A similarly selective high enrichment in DS was observed compared to DP, DF as well as ORS and matrix (Mx) progenitors, and melanocytes (Mc) from P5 follicles[29,35] (Extended Data Fig. 2e).

Finally, we corroborated endothelin receptor mRNA expression in the DS at the protein level. *Ednra*-encoded ET_A and *Ednrb*-encoded ET_B are exclusively expressed in the $ITGA8^+$-marked DS compartment, within murine HFs (Fig. 1i). Overall, these data thus far suggest that endothelin signaling may be engaged as the main pathway in regulating contraction of the DS during follicle regression.

Endothelin receptor activation contracts DS cells *in vitro*

To explore whether endothelin receptor activation in the DS functions to activate cellular contraction, we exposed primary DS cell cultures to endothelin-1 (ET-1) protein *in vitro*. For this, we short-term cultured freshly prepared HF single-cell suspensions from $Acan^{CreERT2};R26^{ACTB\text{-}tdT}$ ($Acan^{tdT}$) mice on matrigel in the presence of ET-1 ligand peptide or vehicle control (Fig. 2a). $Acan^{tdT}$ exclusively labels DS cells in the skin, enabling the identification of DS cells for cell surface area tracing as a measure of contraction status over time[29]. DS cell surface areas in control-treated cells remained unchanged throughout live tracking (Fig. 2b). By contrast, ET-1 exposure strongly reduced DS cell sizes after 60 minutes in a dose-dependent manner down to physiological levels in the nanomolar range (Fig. 2b,c; Extended Data Fig. 3a,b). As ET may also increase cell proliferation, in parallel control experiments we blocked DNA synthesis with mitomycin-C prior to ET-1 addition to rule out obfuscating effects by processes leading up to cell division (Extended Data Fig. 4). ET-1 again caused a significant cell size area reduction already after 5 minutes that continued to increase with time, consistent with cell contraction. These data suggest that ET-1 activates contraction of DS cells that mimics the contraction timing of tonic smooth muscles[40].

Endothelin receptors antagonism *in vivo* impairs HF regression

We next investigated whether the endothelin pathway regulates DS contraction during follicle regression *in vivo*. We hypothesized that if endothelin signaling is the main contraction-activating pathway then pharmacological blocking of ET-1 ligand binding to endothelin receptors should recapitulate regression stalling when the DS contraction machinery is inhibited[29]. To test this, we topically applied endothelin receptor antagonists,

BQ123 (selective for ET_A) and BQ788 (selective for ET_B) to a small back skin region and DMSO control to the contralateral side, twice daily during the follicle regression phase (Fig. 2d). At the subsequent resting phase of the hair growth cycle, full-thickness skin samples were whole-mount immunofluorescence stained and optically cleared for visualizing the basal epithelial marker K14, DS marker ITGA8, and DP marker LEF1 (Fig. 2e). In vehicle control skins, all follicles fully regressed with $LEF1^+$ DP resting adjacent to $K14^+$ hair germ stem cells and $ITGA8^+$ HF dermal stem cells[41] closely enwrapping the DP. In the center of the BQ123/BQ788 treated area, however, we observed a striking failure of follicles to undergo regression (Fig. 2e,f; Extended Data Fig. 5a,b) recapitulating a "stalled regression" phenotype[29]. Abnormally long HFs extended deep into the dermis with DPs situated at the proximal end of follicles and with intact $ITGA8^+$ DS wrapping around the DP and $K14^+$ basal epithelium (Fig. 2e; Extended Data Fig. 5c). Towards the periphery and outside the application area, we observed a progressive decrease in the frequency of stalled follicles (Extended Data Fig. 5d,e), illustrating the local effect of the endothelin receptor inhibitors. To test whether endothelin receptor inhibition also impairs HF regression during the second hair growth cycle, we topically applied endothelin receptor antagonists during second hair cycle regression and again observed many stalled follicles persisting into the second resting phase (Extended Data Fig. 6a–c). Collectively, the *in vivo* pharmacological inhibition experiments demonstrate that endothelin signaling is engaged as a contraction-activating pathway in the DS essential for contraction and follicle regression.

Genetic endothelin receptor ablation stalls follicle regression

Endothelin signaling in vascular smooth muscle cells regulates vasoconstriction and thus pharmacological antagonists applied to the total skin may also affect vascular tone besides inhibiting DS contraction. Therefore, we next investigated the functional role of endothelin signaling exclusively in the DS by genetically ablating the endothelin receptors in the DS. We crossed the $Acan^{CreER}$ driver that specifically targets the DS within the skin[29] with the floxed *Ednra* line ($Ednra^{fl}$) to ablate ET_A[42], the most well studied endothelin receptor regulating vasoconstriction[43,44] (Fig. 3a). Intraperitoneal tamoxifen injection during mid-to-late hair growth (P10-12) – in accordance with our DS genetic targeting protocol[29] – resulted in ET_A ablation by the regression phase. While the $ITGA8^+$ DS robustly expressed ET_A in all follicles of control back skins, many follicles in conditional knockout back skins lacked ET_A expression in the DS, yet surprisingly still appeared to regress normally based on follicle morphology (Fig. 3b; Extended Data Fig. 6d). By the subsequent resting phase, 100% follicles in both control and conditional knockout back skins were fully regressed (Fig. 3c,d). From this we concluded that either ET_A is not the main receptor executing endothelin contraction in the DS and ET_B, which is also highly expressed in the DS (Fig. 1), may instead be the receptor that mediates the activation of DS contraction. To test this, we crossed $Acan^{CreER}$ mice with the $Ednrb^{fl}$ line[45] and utilized the same tamoxifen administration timing as with ET_A (Fig. 3e), which ablated ET_B by the regression phase (Fig. 3f; Extended Data Fig. 6e). As with ET_A single receptor ablation, follicles lacking ET_B appeared to regress normally and were all fully regressed by the resting phase (Fig. 3g,h). Since individually ablating ET_A or ET_B in the DS did not impair HF regression, it suggested that the two endothelin receptors may both be active to regulate regression and be functionally redundant in controlling DS contraction.

We therefore next performed conditional gene ablation of both *Ednra* and *Ednrb* in the DS (Fig. 4a). By the subsequent resting phase when all follicles in control back skins were fully regressed (Fig. 4b), we observed abnormally long follicles that failed to regress (Fig. 4b–d). These "stalled regression" follicles retained hair shafts down to the follicle base with intact ITGA8$^+$ DS wrapping around ITGA9$^+$ DPs at the proximal end of follicles deep in the dermis (Fig. 4e,f). K14$^+$ epithelial progenitors of non-regressed follicles were not undergoing apoptosis or proliferation (Fig. 4g). Stalled follicles were found infrequently but consistently among 100s of follicles in each skin and throughout multiple repeat experiments. To better understand the penetrance of the stalled phenotype in double knockout follicles, we analyzed ET_A/ET_B ablation efficiencies by immunofluorescence for both receptors. Only stalling follicles exhibited high ablation efficiency with >80% of the DS being negative for both receptors (Fig. 4h,i; Extended Data Fig. 7a–c) suggesting that reduced ablation efficiency of either receptor resulted in a lower combined ablation efficiency. Collectively, our DS-specific gene ablation experiments demonstrate that receptors ET_A and ET_B function redundantly to execute endothelin signaling in the DS and that activation of this pathway is required and key for HF regression.

Endothelin-1 from ORS progenitors is required for regression

We next sought to determine the source of the endothelin ligand(s) that bind and activate ET_A and ET_B in the DS to regulate contraction. We reasoned that endothelin signaling activation could be mediated in an autocrine manner wherein DS regulates its own contraction or in a paracrine manner with one or more cell types of the local microenvironment secreting endothelin ligands that signal to the DS (Fig. 5a). Turning to our previously published transcriptome expression data[29,35], we queried expression of the known endothelin ligands *Edn1*, *Edn2*, and *Edn3*. While *Edn3* is exclusively expressed in the DP consistent with its known role in pigmentation regulation[17] (Extended Data Fig. 8a), both *Edn1* and *Edn2* are increased in ORS progenitors (Fig. 5b). Therefore, analogous to how ET-1(*Edn1)* and ET-2 (*Edn2*) secreted by endothelial cells regulate vascular smooth muscle cell contraction in a paracrine fashion[46], we hypothesized that ORS progenitors – ensheathed by and intimately juxtaposed with the DS – are in a prime position to signal to the DS and regulate contraction.

Among the three endothelin ligands, we focused our attention on endothelin-1 (ET-1) encoded by the gene *Edn1* as it is the most potent vasoconstrictor in the mammalian cardiovascular system[43,44]. To assess the spatiotemporal distribution of endothelin ligand gene expression, we first performed single molecule fluorescence *in situ* hybridization (smFISH). Consistent with the RNA-seq data, we observed *Edn1* expression is restricted to the epithelial progenitor population with a robust enrichment in the "bottleneck" region – defined as the interface between the club hair and epithelial strand – where DS contraction is known to occur during regression[29] (Fig. 5c; Extended Data Fig. 8b). At the protein level, we similarly observed ET-1 localization in ITGA6$^+$ K14$^+$ ORS cells with the highest expression in the bottleneck region during middle/late regression (Fig. 5d; Extended Data Fig. 8c). Furthermore, ET-1 appears to be enriched on the side of cells interfacing with the basement membrane separating the DS and progenitors (Fig. 5e). As follicles regress and hair shafts are extruded during middle/late regression, the bottleneck likewise progressively

moves upward and maintains its local enrichment of endothelin ligand (Extended Data Fig. 8c,d). We also observed a corresponding enrichment of phosphorylated myosin light chain (pMYL9) in the DS surrounding and below the bottleneck, consistent with elevated contraction at the bottleneck (Fig. 5f). Collectively, these expression data demonstrate that endothelin ligand ET-1 is produced by the ORS progenitor population in the bottleneck of regressing follicles suggesting that progenitors and DS engage in epithelial-mesenchymal endothelin signaling crosstalk to regulate DS contraction during follicle regression (Fig. 5g).

To functionally test whether progenitor-derived ET-1 regulates DS contraction during follicle regression, we crossed *K14-CreER* mice[47] with the *Edn1*^{fl} line[48] to conditionally ablate *Edn1* in the basal epithelium including the ORS progenitor population (Fig. 6a). We again administered tamoxifen intraperitoneally during mid-to-late follicle growth ablating ET-1 in ORS progenitors by mid-regression (Extended Data Fig. 9). By the following resting phase, many follicles notably failed to regress with stalled follicles throughout the back skin (Fig. 6b,c) similar to ET receptor ablation in the DS. To determine whether ET-1 from the ORS is required for regression also during the second hair cycle, we ablated *Edn1* also during the late growth phase of the second hair cycle (Fig. 6d) and again observed many stalled, aberrantly long follicles that failed to regress (Fig. 6e). This striking result indicates that the epithelial progenitor population in the HF is the main source of ET-1 ligand that is required to control DS contraction during regression.

Endothelin-1 regulates DS contraction via Ca^{2+} levels

Smooth muscle cells in diverse tissues and organ systems mechanistically undergo contraction following cell membrane depolarization or G-protein coupled receptor activation that in turn regulate calcium-dependent pathways that phosphorylate myosin light chain[32,49]. We previously showed that activation of the calcium/calmodulin/myosin light chain kinase pathway (MLCK) is an intracellular mechanism by which the DS contracts[29]. To determine whether endothelin pathway activation in DS cells functions through calcium-dependent pathways to facilitate MLCK activation, we short-term cultured *Acan*^{tdT}-marked DS cells in the presence of Fluo8 Ca^{2+} indicator to assay intracellular Ca^{2+} changes following endothelin pathway activation (Fig. 7a). While in vehicle control conditions intracellular Ca^{2+} remained stable in DS cells, exposure to exogenous ET-1 led to progressive Ca^{2+} increase in DS cells (Fig. 7b; Extended Data Fig. 10a). Increased Ca^{2+} levels were ~50% attenuated by pharmacological antagonism of either ET_A or ET_B with BQ123 or BQ788, respectively. Only dual blocking of both ET_A and ET_B receptors fully abrogated ET-1 induced Ca^{2+} increase (Fig. 7b,c; Extended Data Fig. 10a). This suggests that both receptors are engaged by ET-1 to a similar extent and that ET-1 signals in DS through a calcium-dependent mechanism.

Finally, we asked whether ET-1 induced contraction in the DS requires calcium-dependent signaling or alternative calcium-independent pathways[40,49] may be activated. For this, we preincubated DS cells with a combination of pharmacological inhibitors of cell membrane and sarcoplasmic reticulum calcium channels prior to exogenous ET-1 exposure (Fig. 7d). While ET-1 stimulation in control DS cells again reduced cell areas within 30 minutes (Fig. 7e,f; Extended Data Fig. 10b), preincubation with calcium channel blockers resulted

in a significant block of DS cell contraction, similar to preincubation with myosin light chain kinase inhibitor ML7 (Fig. 7e,f; Extended Data Fig. 10b). Taken together, this illuminates a Ca^{2+}-dependent mechanism by which ET-1 signals in DS cells. Overall, these data demonstrate that endothelin signaling in the DS operates equally and functionally redundantly through ET_A and ET_B, triggering mobilization of extracellular (via L-type and T-type channels) and intracellular (via IP3R and RyR channels) calcium stores to activate the Ca^{2+}/calmodulin/MLCK pathway, thereby controlling DS contraction and HF regression.

DISCUSSION

In the present study, we sought to decipher the precise molecular signals that control the dynamic contraction of a functional smooth muscle, the dermal sheath, during the drastic follicle reorganization in the regression phase of the hair growth cycle. We executed transcriptomic analysis of the DS in comparison to the DP and dermal fibroblasts, during the transition from tissue growth to regression. From this analysis, we identified endothelin signaling, which is one of the most studied and prominent regulatory pathways of vascular tone and blood flow by balancing vasoconstriction and vasodilation[43,44], as a potential DS contraction-activating pathway. Subsequently, functional pharmacological and genetic manipulations of endothelin receptors established the requirement for endothelin signaling in DS contraction and HF regression. Spatiotemporal examination of endothelin ligand mRNA and protein expression then uncovered dynamic regulation of endothelin-1 in the ORS progenitor population, and that ORS-derived ET-1 is a main source of endothelin ligand that triggers DS contraction via cytoplasmic calcium influx through calcium channels of the plasma membrane and sarcoplasmic reticulum (summary schematic in Fig. 7g). We propose an overall “rolling wave” model for hair follicle regression wherein (1) the epithelial progenitors of the club hair/epithelial strand bottleneck produce high levels of ET-1 ligand that induces local DS contraction and (2) that as regression progresses the bottleneck moves continuously up the regressing follicle in a “rolling wave” fashion to extrude the hair shaft and relocate the DP (Fig. 7h).

It will be interesting to parse in future studies the mechanism(s) that control the dynamic transcriptional regulation of *Edn1* in the ORS progenitors, predominantly located at the dying epithelial strand/club hair bottleneck. A plethora of key transcription factors are known to regulate *Edn1* expression[50], and it will be important to dissect the specific transcription factor networks underpinning the spatiotemporal regulation in the ORS as well as the cell-intrinsic and extrinsic factors influencing these transcription factors’ expression control. Another interesting line of investigation that our results invite is endothelin ligand redundancy in the regulation of DS contraction and hair cycle progression. We observed enrichment of *Edn2* in ORS progenitors in concert with *Edn1*, and ET-2 is also known for its potent vasoconstricting capacity as well as inducing smooth muscle contraction in other organ systems[51–53], raising the distinct possibility of cooperative activation of endothelin receptors by both ligands during HF regression. It is equally conceivable that ET-1 derived from endothelial cells of the condensing vasculature close to regressing HFs[54] could contribute to DS contraction. Nevertheless, the robust phenotype of stalled HFs in the epithelial ET-1 ablations suggests that ET-1 from progenitors is the major ligand and source.

Our endothelin receptor expression and gene ablation experiments revealed both ET_A and ET_B as robustly expressed and functioning redundantly in the DS. They also suggest that both receptors are constitutively active during regression given that single receptor knockouts did not show a stalled regression phenotype, although we cannot rule out additional compensatory upregulation of the remaining other receptor. In this context another interesting aspect is a potential cooperativity between ET_A and ET_B receptors that could lead to increased DS contraction activity, similar to elevated blood pressure following combined ET receptor knockout in renal collecting ducts[55].

Endothelin-induced contraction has a vast array of functions in diverse organ systems and here we reveal yet another system that depends upon endothelin-induced contraction: homeostatic tissue turnover in the hair follicle. Overall, our findings support a model wherein HF progenitors regulate the contraction of the DS smooth muscle, which in turn facilitates coordinated tissue regression to achieve homeostasis. Analogous to endothelial cells of the vasculature secreting endothelin to induce vascular smooth muscle contraction[46], the epithelial cells of the HF secrete ET-1 which functionally induces contraction of proximally positioned DS smooth muscle. Notably, ET-1 upregulation is transient, occurring primarily during the mid-regression stages to induce the contraction that extrudes the hair shaft from the skin. Interestingly, a similar paradigm also unfolds in the ovary, where *Edn2* is transiently upregulated in granulosa cells immediately prior to ovulation and is required for ET-2–ET_A dependent intraovarian contraction that triggers oocyte expulsion[53,56,57]. It is tempting to speculate that similar mechanisms may exist in other organ systems as well.

Endothelin is known for being mitogenic for epithelial tissues in the context of cancer[58–60], but here it surprisingly serves a functionally opposite role, contributing to the degeneration of the epithelium rather than expansion. Intriguingly, epithelial progenitors of the HF regulate their own fate through an epithelial-mesenchymal feedback loop, secreting the endothelin ligands that triggers contraction fueling tissue involution and reduction of the progenitor pool. Future studies may reveal whether endothelin-induced contraction also regulates other hair cycle phases, such as inducing the transition from growth to regression. Epithelial-mesenchymal feedback loops orchestrate tissue homeostasis across a variety of systems, including the intestinal and lung epithelial stem cell niches[61,62], and it has become evident in recent years that stem cells and progenitors are indeed “architects” of the niche in which they reside[3]. Our findings highlight that this holds true beyond tissue regeneration and is also a key principle underlying stem cell niche remodeling during tissue regression that counterbalances growth to achieve homeostasis.

METHODS

Mice and experimental conditions

Acan^{CreER} [63] and *R26*$^{LSL\text{-}tdTomato}$ (Ai14)[64] were obtained from the Jackson Laboratory. *K14-CreER* mice[47] were generously provided by Elena Ezhkova, and *Ednra*^{fl} [42], *Ednrb*^{fl} [45], and *Edn1*^{fl} [48] lines by David Pollock and Ilse Daehn. *Tbx18*^{H2BGFP}, *Crabp1-GFP, K14*^{H2BGFP} and *Lef1-RFP*[16,33–35] mice used to label key skin populations were described previously. *Acan*^{CreER};*R26*$^{LSL\text{-}tdTomato}$, *Acan*^{CreER};*Ednra*$^{fl/fl}$, *Acan*^{CreER};*Ednrb*$^{fl/fl}$, *Acan*^{CreER};*Ednra*$^{fl/fl}$;*Ednrb*$^{fl/fl}$ and *K14-CreER/Edn1*$^{fl/fl}$ mice were

injected with tamoxifen (20mg/ml dissolved in corn oil, injections of 0.15g/kg body weight i.p.) daily from P10-P12 for DS-labeling and DS endothelin receptor or progenitor ligand ablation experiments during the first hair growth cycle. For second hair cycle ligand ablations, 0.5 mg 4-OHT in ethanol and ethanol control were topically applied for 3 days in shaved 1 x 1 cm regions or 10 μg 4-OHT were intradermally spot-injected for 3 days in 4 separate regions per mouse. Animals were PCR genotyped to select for control and experimental groups. All labeling and ablation experiments were repeated with at least three different mice; all specific *n* values for each experiment are listed in figure legends. All mice used in this study were housed in an environmentally controlled vivarium, at 22 °C and 50-60 % humidity on a 12h:12h reversed light/dark cycle, with food and water available *ad libitum,* operated by the Center for Comparative Medicine and Surgery (CCMS) at ISMMS. Mice from experimental and control groups were randomly selected for all experiments. No blinding was done as all mice were genotyped prior to experiments and no data were excluded from the analyses. All animal studies were conducted in accordance with the guidelines and approval of the Institutional Animal Care and Use Committee (IACUC) at ISMMS under protocol number 08-0452.

Immunofluorescence and microscopy

For immunofluorescence of tissue sections, back skins were harvested and embedded in OCT (Tissue Tek) before sectioning with 7 μm thickness with a Leica cryostat. Slides were thawed and post-fixed with 4% paraformaldehyde for 10 minutes at room temperature. Sections were then washed in 0.1% Tween 20/PBS solution and permeabilized in 0.3%-1.0% Triton X-100/PBS for 15 minutes at room temperature. Blocking was performed using 0.5% normal donkey serum (Jackson ImmunoResearch) and 1% bovine serum albumin (Sigma Aldrich) or MOM blocking reagent for mouse primary antibodies (Vector Labs) for 1 hour at room temperature or overnight at 4 °C, respectively. Primary antibody labeling was also performed for 1 hour at room temperature or overnight at 4 °C. Primary antibodies used in this study were (Supplementary Table 2): ITGA8 (R&D Systems, goat 1:100), ITGA9 (R&D Systems, goat 1:100), K14 (Biolegend, 1:500), activated CASP3 (R&D Systems, rabbit 1:300), Ki67 (Abcam, 1:500), pH3 (Abcam, 1:1000), ITGA6 (Santa Cruz, goat 1:100), ET_A (Thermo Fisher, 1:500), ET_B (Abcam, 1:500), ET-1 (Thermo Fisher, 1:100), GFP (Milipore, 1:1000), RFP (Abcam, 1:200), αSMA (Abcam, 1:300), pMYL9 (Invitrogen, 1:250). Secondary antibody labeling was done with donkey anti-goat, rabbit, rat or mouse antibodies conjugated with AlexaFluor 488, 555, or 647 (Jackson ImmunoResearch, Invitrogen, 1:400) (Supplementary Table 2) for 30 minutes at room temperature. Nuclei were labeled with Hoechst 33342 (Thermo Fisher, 1:1000), and stained sections were mounted in glycerol-based p-phenylenediamine (Sigma) antifade reagent. Whole mount immunofluorescence of pieces of intact back skin followed a previously published protocol[65] with modifications as recently described[29]. Briefly, tissues were harvested and fixed in 4 % PFA for 2 hours at room temperature or overnight at 4°C before peeling off the panniculus carnosus muscle and cutting 1 cm x 2 cm strips. Skins were permeabilized with 0.3 % Triton X-100/PBS for 5-8 hours before primary antibody staining for K14 (rabbit 1:1000) in a 0.3 % Triton X-100, 5 % donkey serum, 20 % DMSO/PBS solution at room temperature for 3-5 days with gentle shaking in 6-well plate wells. After washing in 0.3 % Triton X-100/PBS solution for 5-8 hours at room temperature with buffer

changes every 30 minutes, tissues were stained with a donkey anti-goat AlexaFluor 488/555 antibody in Triton X-100/donkey serum/DMSO/PBS for 2-3 days at room temperature with gentle shaking. Tissues were washed in 0.3 % Triton X-100/PBS for 5-8 hours at room temperature with buffer changes every 30 minutes and stained with Hoechst 33342. Optical clearing was performed by dehydration in 50:50 methanol/water for 5 minutes followed by a series of 3x 100% methanol for 30 minutes at room temperature. The final clearing step was in BABB (benzyl alcohol/benzyl benzoate, 1:2 ratio) until visibly clear and then the tissues were mounted in residual BABB in a chambered glass slide. Epifluorescence microscopy was performed using the Leica DM5500 widefield microscope, while confocal microscopy was performed with a Leica SP5 DMI confocal microscope equipped with Leica LASAF software. Images were post-processed and adjusted for levels, brightness and contrast using ImageJ/FIJI (NIH).

Single-molecule mRNA fluorescence *in situ* hybridization

Single-molecule mRNA fluorescence in situ hybridization (smFISH) was performed on 7 μm thick cryo-sections of P17 back skins using RNAscope (Advanced Cell Diagnostics) according to the manufacturer's instructions. Briefly, back skins were fixed in 4% PFA, dehydrated through a graded methanol (MeOH) series (50%, 70% and 100% MeOH/H_2O), and stored at −20 ° C overnight in 100% MeOH. Skins were rehydrated and pretreated with hydrogen peroxide and protease III (2.5 HD Reagent Kit-RED), and hybridized with an *Edn1* probe (ACD #435221, Supplementary Table 2) overnight at 40 °C. Skins were washed, postfixed in 4% PFA for 15 minutes at room temperature, followed by signal amplification with hybridizing horseradish peroxidase-labeled probes and fast red signal detection, as described in the manufacturer's kit instructions. Slides were then imaged as described above. The red chromogenic substrate was visualized as autofluorescence in the red fluorescent channel.

Isolation of DS, DP, and DF

Back skins were harvested from P16 mice and digested in dispase (Invitrogen) overnight at 4 °C. and the dermis was then digested in a 0.2% collagenase (Sigma-Aldrich) and DNase (20 U/μl, Roche) solution at 37 °C for one hour with gentle shaking. Cell pellets were obtained by centrifugation at 300 x g for 10 minutes and further digested in 0.25 % trypsin EDTA solution for 5 minutes at 37 °C. Cells were then stained against ITGA8 (R&D Systems, goat 1:50) and PDGFRA (eBiosciences, biotinylated rat, 1:50,) followed by donkey anti-goat-APC and streptavidin-Brilliant Violet 421 (Biolegend, 1:200) secondary staining. DAPI was added for live/dead cell identification and cells were sorted using a BD Influx cell sorter at the ISMMS Flow Cytometry Core facility.

$Tbx18^{H2BGFP}$;Crabp1-GFP;Lef1-RFP reporter mice were used to purify simultaneously DS, DP and DF. GFP was expressed in DP (*Crabp1-GFP* high) and DS (*$Tbx18^{H2BGFP}$* high). DP and DS were distinguished based on RFP expression in DP. DS was further purified by selection as ITGA8-APC$^+$, PDGFRA-Brilliant Violet 421$^+$. The following criteria was used to sort each population: DP = GFP$^+$, RFP$^+$, ITGA8$^-$, PDGFRA$^+$; DS = GFP$^+$, RFP$^-$, ITGA8$^+$, PDGFRA$^+$; DF = GFP$^-$, RFP$^+$, ITGA8$^-$, PDGFRA$^+$. FACS profiles were analyzed using FlowJo software.

qRT-PCR

Whole cell RNA was purified from sorted cells using the Absolutely RNA Nanoprep Kit (Agilent). cDNA synthesis was done with Superscript III (Invitrogen) using oligo(dT) primers. qRT-PCR was performed using SYBR Green Master Mix I (Roche) on a LightCycler 480 thermocycler (Roche). Relative mRNA levels were calculated using the $2^{-\Delta\Delta Ct}$ method, normalized to *Gapdh*. All measurements were performed with biological duplicates each with technical duplicates. Gene specific primers are listed in Supplementary Table 3.

RNA sequencing and analysis

RNA purification and bulk RNA-sequencing were performed as previously described[29,36]. Briefly, total RNA was purified from sorted cells with the Absolutely RNA Nanoprep Kit (Agilent). RNA concentrations were measured with a NanoDrop spectrophotometer (Thermo), and quality was assessed with an Agilent Bio-analyzer. Samples with RNA integrity number score ≥8 were further processed. 6 ng of starting material was reverse transcribed and amplified with the RNA Ovation RNAseq System V2 (NuGEN). cDNA was sheared with a Covaris LE220 sonicator. From 100 ng of sheared amplified cDNA, sequencing libraries were generating with 6 unique barcoded adaptors, one for each sample (2 biological replicates x 3 populations) using the Ovation Ultralow DR Library System (NuGEN). Library concentration and quality were quantified by Qubit (Invitrogen) and Agilent Bioanalyzer. Samples were then sequenced on the Illumina HiSeq 2000 platform using a 50-nt single-read setting at the Genome Technology Center at NYU.

Raw RNA sequencing reads were mapped to reference genome sequence GRCm39, transcript version M25 with Salmon v1.9.0[66]. Transcriptomes were imported and assembled using tximport and the DESeq2 pipeline[67]. Reads per kilobase per million (RPKM) reads mapped for each gene were computed with DESeq2 1.28.1 using raw counts and avgTxLength. Differentially expressed genes (DEGs) were identified using DESeq2 with default parameters and applying adjusted p-values with a Benjamini-Hochberg correction for multiple hypothesis testing and a significance cut off of < 0.05. Principal component analysis was performed on regularized-logarithm transformed counts of the top 2500 genes using DESeq2. Hierarchical clustering analysis was performed with Morpheus (Broad Institute, https://software.broadinstitute.org/morpheus) using RPKM expression levels of the top 2500 DEGs and a Pearson correlation metric. Population signature genes were defined by DEGs with an RPKM ≥ 1, and fold enrichment ≥ 2 compared to all other populations. Our previously published combined analysis of DS, DP, and DF gene signatures[29] and of those of HF outer root sheath, matrix, and melanocytes obtained at the same age P5[35] were also surveyed for expression of smooth muscle contraction receptors as well as endothelin signaling pathway components. Gene ontology analysis was performed using Enrichr (Ma'ayan Lab)[68] using the GO Biological Process gene set database.

In vitro DS contraction and cytoplasmic Ca^{2+} assays

DS was fluorescently labeled using $Acan^{CreER}$ mice crossed with $R26^{LSL\text{-}tdTomato}$ with intraperitoneal tamoxifen injections occurring at P10 and P11. P14 back skins were harvested from which single cell suspensions were prepared as described above for flow

isolations and plated into 12-well plates. Cells were grown at 37° C and 5% CO_2 in DMEM (Gibco) with 10% bovine calf serum (HyClone) for 48 hours prior to the assay with a media swap halfway through the incubation at 24 hours post-plating. 1 hour prior to the assay, media was exchanged for Krebs buffer + glucose and cells were incubated again at 37° C and 5% CO_2 until the start of the assay. During this 1-hour incubation, cells were preincubated with either vehicle control (DMSO), BQ123 (1 μM), BQ788 (1 μM), or BQ123 + BQ788 for the cytoplasmic [Ca^{2+}] assays, and cells were preincubated with either ML7 HCl (Tocris, 200 μM) or a cocktail of (NNC 55-0396 (50μM) + Diltiazem (50μM) + Ryanodine (10μM) + Xestospongin C (10μM). Mitomycin C (Sigma) was used at a concentration of 4 ug/mL with a 4-hour incubation prior to the swap to Krebs buffer + glucose. DS cells were identified for analysis by tdTomato fluorescence. At the onset of imaging, media was exchanged for fresh Krebs buffer + glucose containing ET-1 (R&D Systems, 1 μM).

Both assays were imaged using an inverted DM6000 microscope with an enclosed live cell chamber at 37 °C and 5% CO_2. For the contraction assays, plates were pre-coated with Matrigel (Corning, 354230,1:50), and cell surface areas were measured in FIJI by quantifying areas of thresholded fluorescence signal exclusive of cell-occupied areas. For the cytoplasmic Ca^{2+} assays, the Fluo8 No-wash Calcium Assay Kit (AAT Bioquest) was used according to the manufacturer's protocol except with Krebs buffer + glucose instead of Hanks' buffer with 20 mM HEPES, and fluorescence intensity was measured in FIJI by averaging the mean pixel intensity of three 20 x 20-micron areas per cell. The researcher quantifying both cell surface area and fluorescence intensity was blinded for all measurements.

In vivo endothelin receptor antagonism

Two regions on contralateral sides of the dorsal back skins measuring 0.5 x 0.5 cm were closely clipped during the late growth phase of the first and second hair cycle before topical BQ123 + BQ788 (Sigma Aldrich) or vehicle control application. 20 μl of BQ cocktail (50 μM each in DMSO) were pipetted onto the clipped regions and locally rubbed into the skin using a glass cell spreader rod for about 30 seconds. Following each topical application each mouse was single housed for about 30 minutes until application sites were visibly dry. Topical applications were performed twice daily separated by 12 hours. 1 x 1 cm regions of back skins were harvested at P20 for downstream analysis to include treated areas in the center with 0.25 x 0.5 cm regions outside the application area to the anterior and posterior.

Statistics and reproducibility

Data are represented as percentages or bar plots with error bars as mean ± s.d. Two-tailed unpaired Student's *t*-test was used to analyze data sets with two groups. One-way ANOVA followed by Tukey's HSD test to adjust for multiple pairwise comparisons were used to analyze data sets with >2 groups. Generation of data plots and statistical analyses were performed using Microsoft Excel. No statistical method was used to predetermine sample sizes, but sample sizes are similar to those reported in previous studies[29,33,35,36]. Data distribution was assumed to be normal. As it was not formally tested all the individual data points were shown. *P* values < 0.05 were designated as significant and symbolized in figure

plots as *$P < 0.05$, **$P < 0.01$, ***$P < 0.001$. Exact P values for Fig. 7c are as follows: **$P = 0.0012$ (ET-1), 0.0016 (ET-1 + BQ788) at 5 min; 0.0027 (ET-1 + BQ123) at 10 min. ***$P = 3.38 \times 10^{-10}$ (ET-1), 5.68×10^{-7} (ET-1 + BQ788) at 10 min; 1.12×10^{-13} (ET-1), 0.0002 (ET-1 + BQ123), 5.68×10^{-7} (ET-1 + BQ788) at 20 min; 1.19×10^{-14} (ET-1), 5.21×10^{-7} (ET-1 + BQ123), 4.59×10^{-9} (ET-1 + BQ788) at 30 min. P values for Fig. 7f are: ***$P =$ 0.0004, 5.30×10^{-5}, 4.79×10^{-7}, 2.78×10^{-6} at 5, 10, 20, 30 min for ET-1 compared to control.

Extended Data

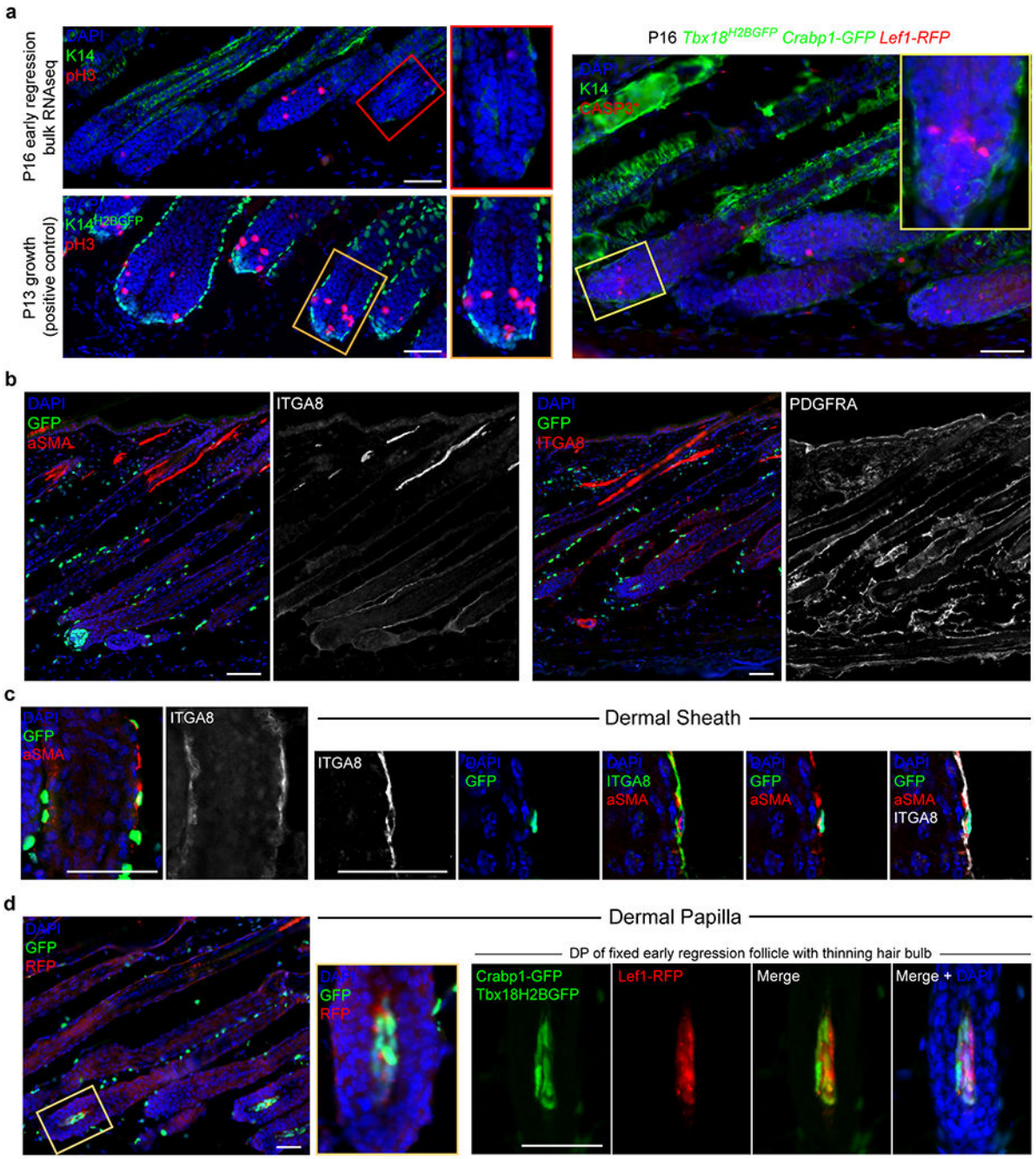

Extended Data Fig. 1. Validation of DS, DP and DF isolation strategy during the growth-to-regression transition

a, Immunofluorescence for pH3 and CASP3* on P16 *Tbx18^{H2BGFP};Crabp1-GFP; Lef1-RFP* reporter mouse back skin (n = 2 mice). P13 anagen back skin served as a positive control for pH3. In the hair bulb, proliferation is decreasing and apoptotic cells are beginning to appear, indicating the growth-to-regression transition. Scale bars, 50 μm. **b**, Immunofluorescence for aSMA, PDGFRA and ITGA8 on P16 *Tbx18^{H2BGFP};Crabp1-GFP;Lef1-RFP* reporter mouse

back skin (n = 2 mice). Scale bars, 50 μm. **c**, Immunofluorescence for ITGA8, aSMA, and GFP on P16 *Tbx18^{H2BGFP};Crabp1-GFP;Lef1-RFP* reporter mouse back skin, demonstrating colocalization in the dermal sheath (n = 2 mice). Scale bars, 50 μm. **d**, Immunofluorescence for GFP and RFP on fresh frozen and fixed P16 *Tbx18^{H2BGFP};Crabp1-GFP;Lef1-RFP* reporter mouse back skin, both demonstrating colocalization in the DP (n = 2 mice). Scale bars, 50 μm.

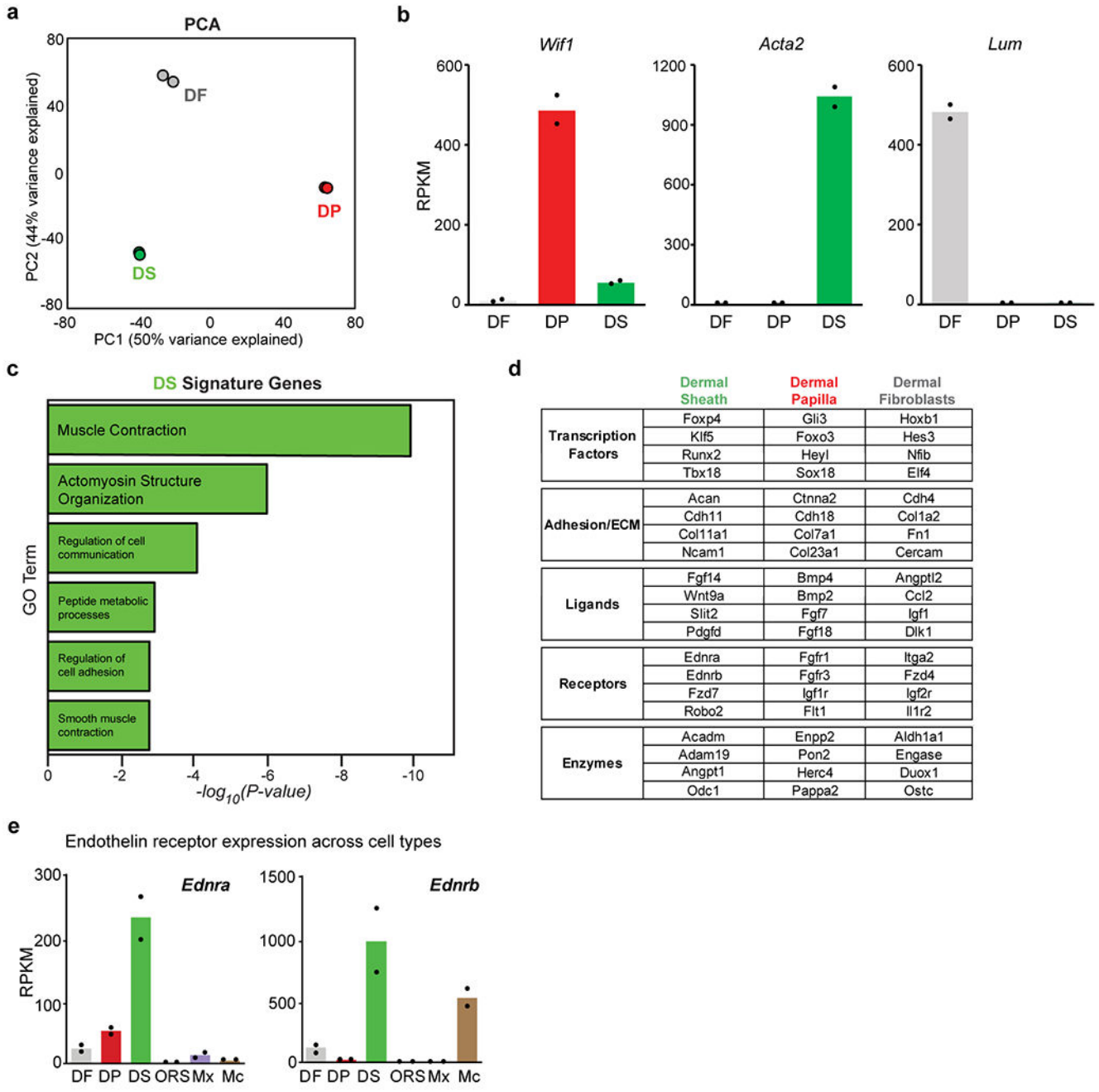

	Dermal Sheath	Dermal Papilla	Dermal Fibroblasts
Transcription Factors	Foxp4	Gli3	Hoxb1
	Klf5	Foxo3	Hes3
	Runx2	Heyl	Nfib
	Tbx18	Sox18	Elf4
Adhesion/ECM	Acan	Ctnna2	Cdh4
	Cdh11	Cdh18	Col1a2
	Col11a1	Col7a1	Fn1
	Ncam1	Col23a1	Cercam
Ligands	Fgf14	Bmp4	Angptl2
	Wnt9a	Bmp2	Ccl2
	Slit2	Fgf7	Igf1
	Pdgfd	Fgf18	Dlk1
Receptors	Ednra	Fgfr1	Itga2
	Ednrb	Fgfr3	Fzd4
	Fzd7	Igf1r	Igf2r
	Robo2	Flt1	Il1r2
Enzymes	Acadm	Enpp2	Aldh1a1
	Adam19	Pon2	Engase
	Angpt1	Herc4	Duox1
	Odc1	Pappa2	Ostc

Extended Data Fig. 2. Analysis of DP, DS, and DF transcriptomes at the growth-to-regression transition

a, Principal components analysis of P16 DS, DP, and DF bulk RNA-sequencing data. **b**, DF, DP and DS RPKM expression levels of *Wif1, Acta2* and *Lum* at regression onset ($n = 2$, data are mean with individual data points). **c**, Gene ontology terms enriched in the DS population. “Muscle contraction” is the top enriched GO term for the DS. $P < 0.05$, Fisher’s exact test. **d**, Transcription factors, adhesion/ECM molecules, ligands, receptors, and enzymes that are part of the gene signatures of the DS, DP and DF populations. **e**, Expression of endothelin receptors across cell types from previously published transcriptome data at P5[20,32]($n = 2$, data are mean with individual data points).

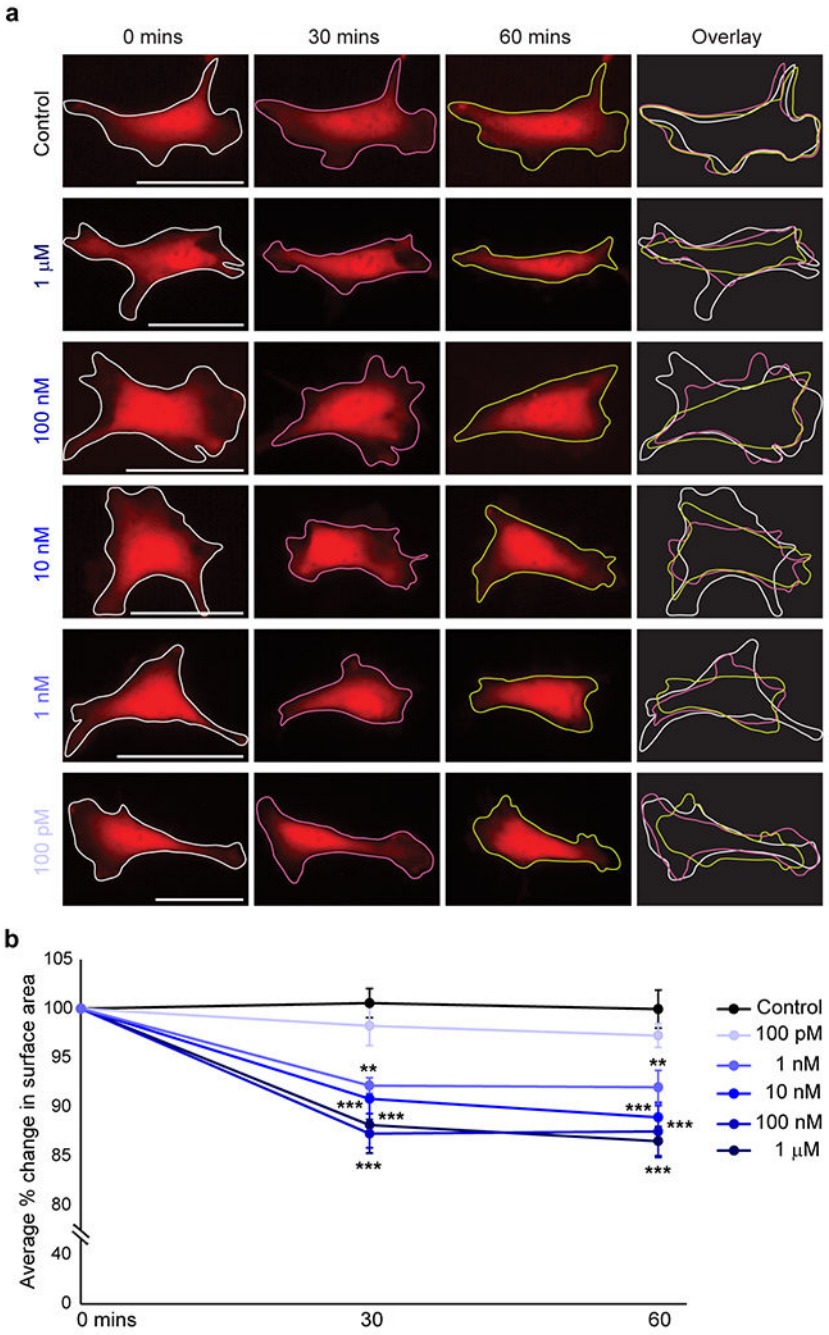

Extended Data Fig. 3. Endothelin signaling contracts DS cells in a dose-dependent manner

a, Endothelin-1 (ET-1) triggers DS contraction and surface area reduction in DS cells grown on Matrigel in a dose-dependent manner. Scale bars, 50μm. **b**, Quantification of cell surface areas during contraction time course (0, 30, and 60 minutes). 24, 20, 21, 18 and 19 cells for control, 100 pM, 1 nM, 10 nM, 100 nM and 1uM ET-1, respectively; $n = 3$ independent experiments. $^{**}P = 0.001$ (30 min) and 0.002 (60 min) for 1 nM ET-1. $^{***}P = 0.00027$ (30 min) and 8.65×10^{-5} (60 min) for 10 nM ET-1, 1.24×10^{-5} (30 min) and 2.5×10^{-5} (60 min) for 100 nM ET-1, and 2.53×10^{-5} (30 min) and 1.14×10^{-5} (60 min) for 1 μM ET-1.

Data are mean ± s.d. and statistical significance was determined by one-way ANOVA with post-hoc Tukey's HSD for multiple comparison testing.

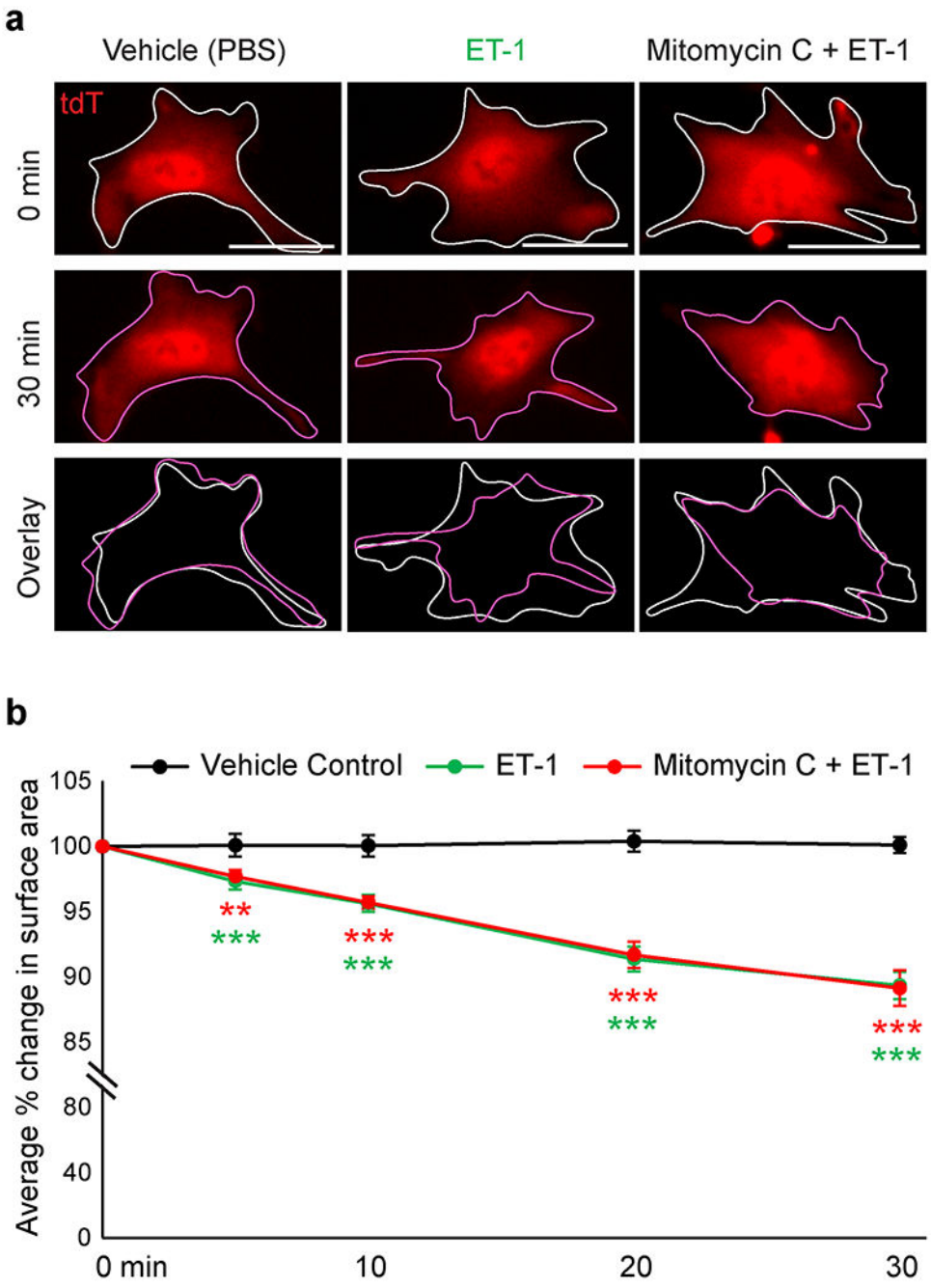

Extended Data Fig. 4. Endothelin signaling functionally contracts DS cells independent of proliferation

a, Endothelin-1 (ET-1) triggers contraction and surface area reduction in DS cells grown on matrigel, both in the absence or presence of proliferation inhibition with Mitomycin-C. Scale bars, 50 μm. **b**, Quantification of cell surface areas during contraction time course. *N* = 19, 20, 19 cells for control, ET-1, Mitomycin C + ET-1, respectively, from two independent

experiments. **P = 0.0015 (5 min) for Mitomycin C + ET-1; ***P = 0.0002 (5 min), 0.0001 (10 min), 1.42 x 10^{-5} (20 mins) and 1.12 x 10^{-5} (30 mins) for ET-1; 0.0002 (10 min), 3.59 x 10^{-5} (20 min) and 61.90 x 10^{-5} (30 min) for Mitomycin C + ET-1. Data are mean ± s.d. and statistical significance was determined by one-way ANOVA with post-hoc Tukey's HSD for multiple comparison testing.

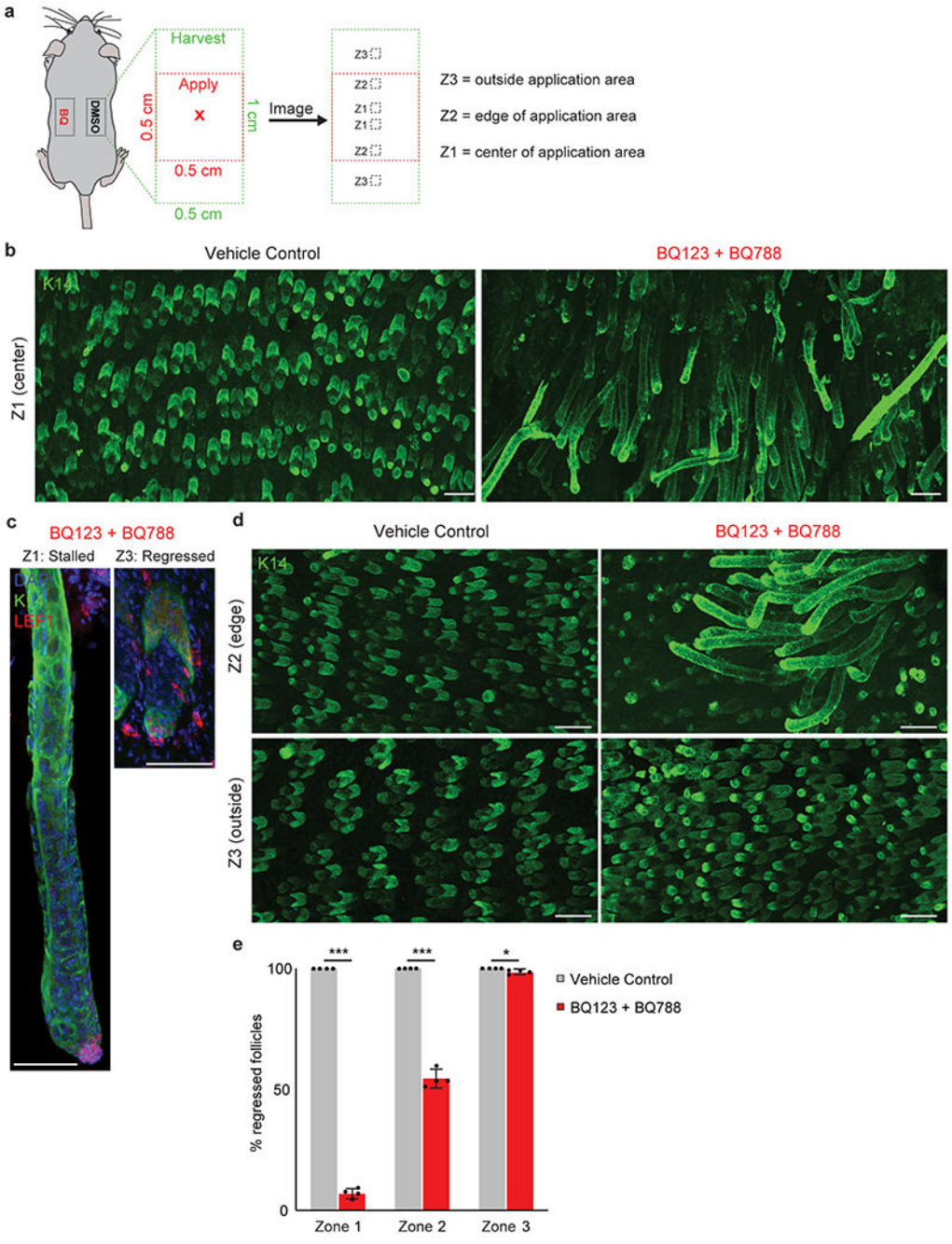

Extended Data Fig. 5. Topical application of endothelin receptor antagonists impedes HF regression with concentrated and local effects

a, Schematic of the experimental design for topical application of endothelin receptor antagonists BQ123 and BQ788 ("BQ") or vehicle control (DMSO), harvesting of the back skins, and imaging strategy. **b**, Whole-mount immunofluorescence for K14 from the center of the application area (Zone 1). Most follicles failed to regress in regions treated with BQ123 + BQ788. Scale bars, 50 μm. **c**, Whole-mount immunofluorescence for K14, LEF1, and DAPI showing a stalled follicle from Zone 1 and a regressed follicle from Zone 3 of BQ123 + BQ788 treated back skin. Scale bars, 50 μm. **d**, Whole-mount immunofluorescence for K14 at the edge (Zone 2) and just outside of (Zone 3) the application area, demonstrating a progressive decline in stalled follicles towards the periphery. Scale bars, 50μm. **e**, Quantification of stalled HFs from each of the three zones. 1200 follicles per zone for vehicle control; 938, 841, and 1087 follicles for Zone 1, 2, and 3, respectively, in BQ123 + BQ788 treated regions; $n = 4$ mice). $*P = 0.0228$ (Zone 3), $***P = 1.69 \times 10^{-10}$ (Zone 1) and 2.42×10^{-7} (Zone 2), unpaired two-tailed Student's *t*-test. Data are mean ± s.d. with individual data points.

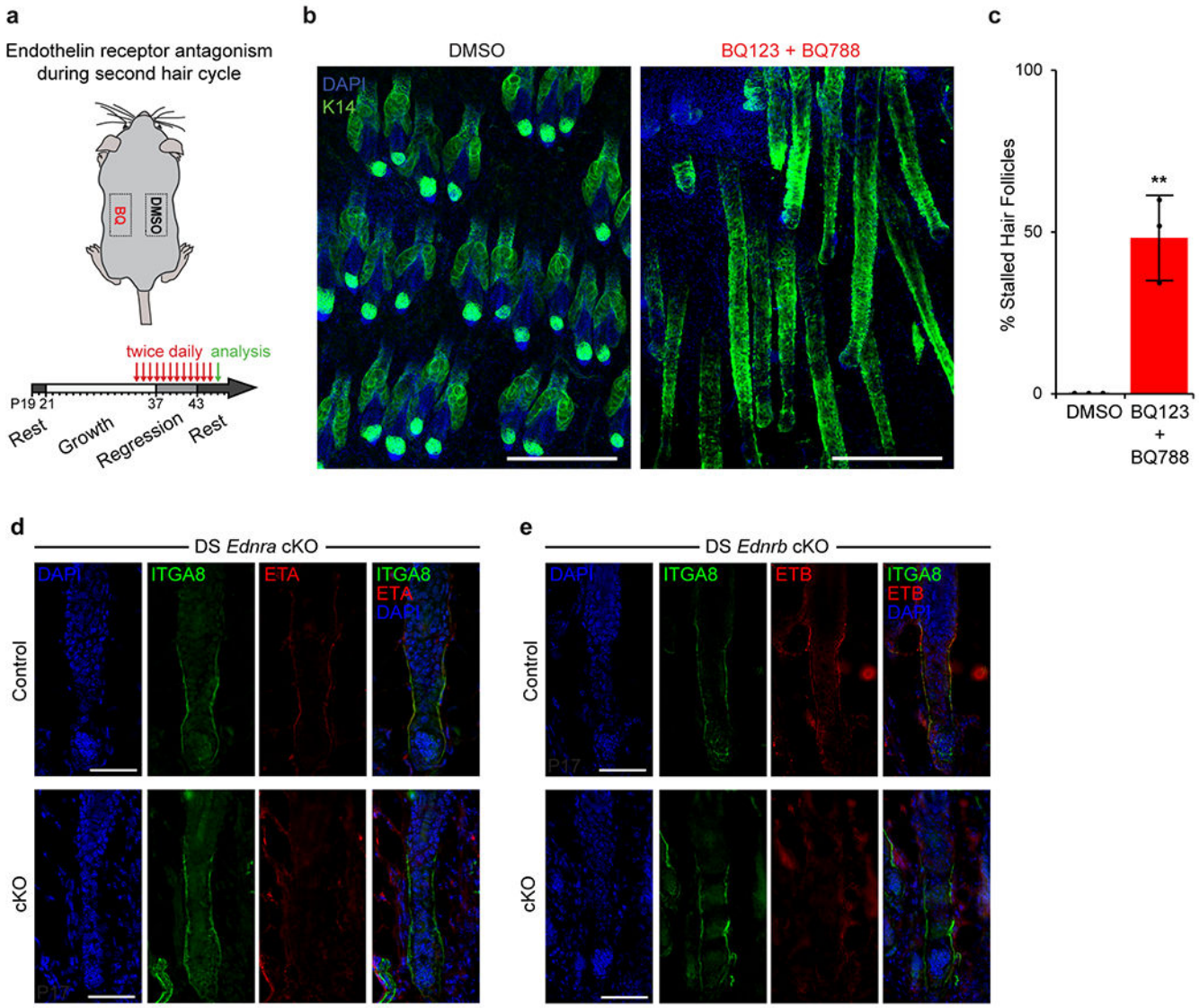

Extended Data Fig. 6. Topical application of endothelin receptor antagonists impedes follicle regression during the second hair cycle

a, Schematic of the experimental design for topical application of endothelin receptor antagonists BQ123 and BQ788 ("BQ") or vehicle control (DMSO), harvesting of the back skins, and imaging strategy. **b**, Whole-mount immunofluorescence for K14 and DAPI in DMSO (vehicle control) and BQ123 + BQ788 treated back skin. Scale bars, 200 μm. **c**, Quantification of stalled HFs observed in DMSO (vehicle control) and BQ123 + BQ788 treated back skins. 924 follicles for DMSO and 544 follicles for BQ123 + BQ788, n = 3 mice. $^{**}P = 0.0031$, unpaired two-tailed Student's t-test. Data are mean ± s.d. with individual data points. **d**, DS-specific *Ednra* ablation at P17. Low magnification image of the follicle from the high magnification image in Fig. 3b. **e**, DS-specific *Ednrb* ablation at P17. Low magnification image of the follicle from the high magnification image in Fig. 3E. Scale bars, 50 μm.

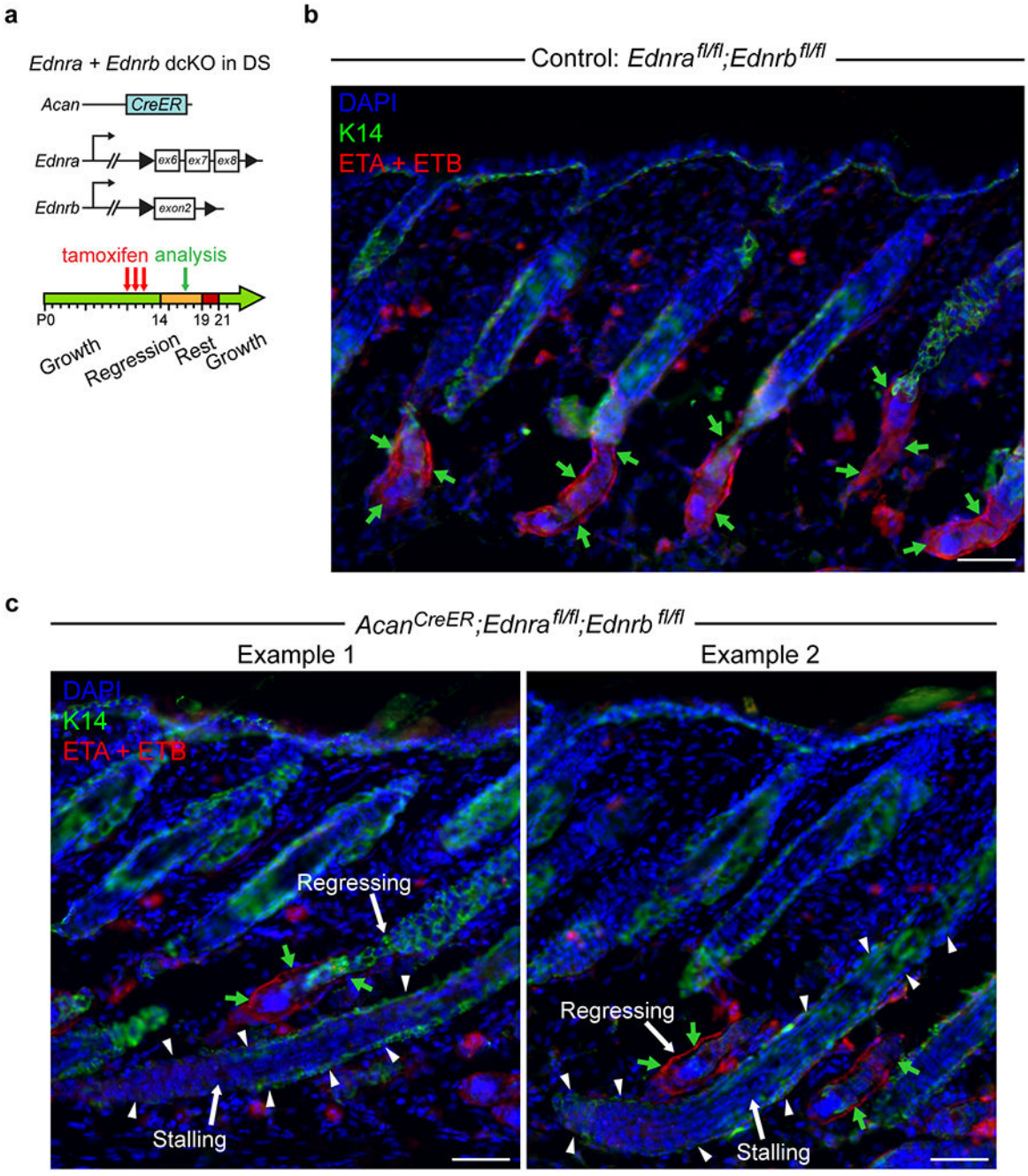

Extended Data Fig. 7. Stalling follicles, but not regressing follicles, in dcKO back skin lack both ET_A and ET_B receptors

a, Schematic of DS-specific *Ednra* and *Ednrb* double conditional genetic ablation (dcKO) in the skin. **b**, Immunofluorescence for K14 and both ET_A/ET_B in control P17 back skins. Endothelin receptors are expressed in the DS. **c**, Immunofluorescence for K14 and both ET_A/ET_B in DS-specific dcKO P17 back skin. Only stalling follicles lack both receptors ET_A and ET_B in the DS. Scale bars, 50 μm. $n = 4$ mice. Green arrows = presence of ET_A and/or ET_B in the DS. White arrowheads = lack of both ET_A and ET_B in the DS.

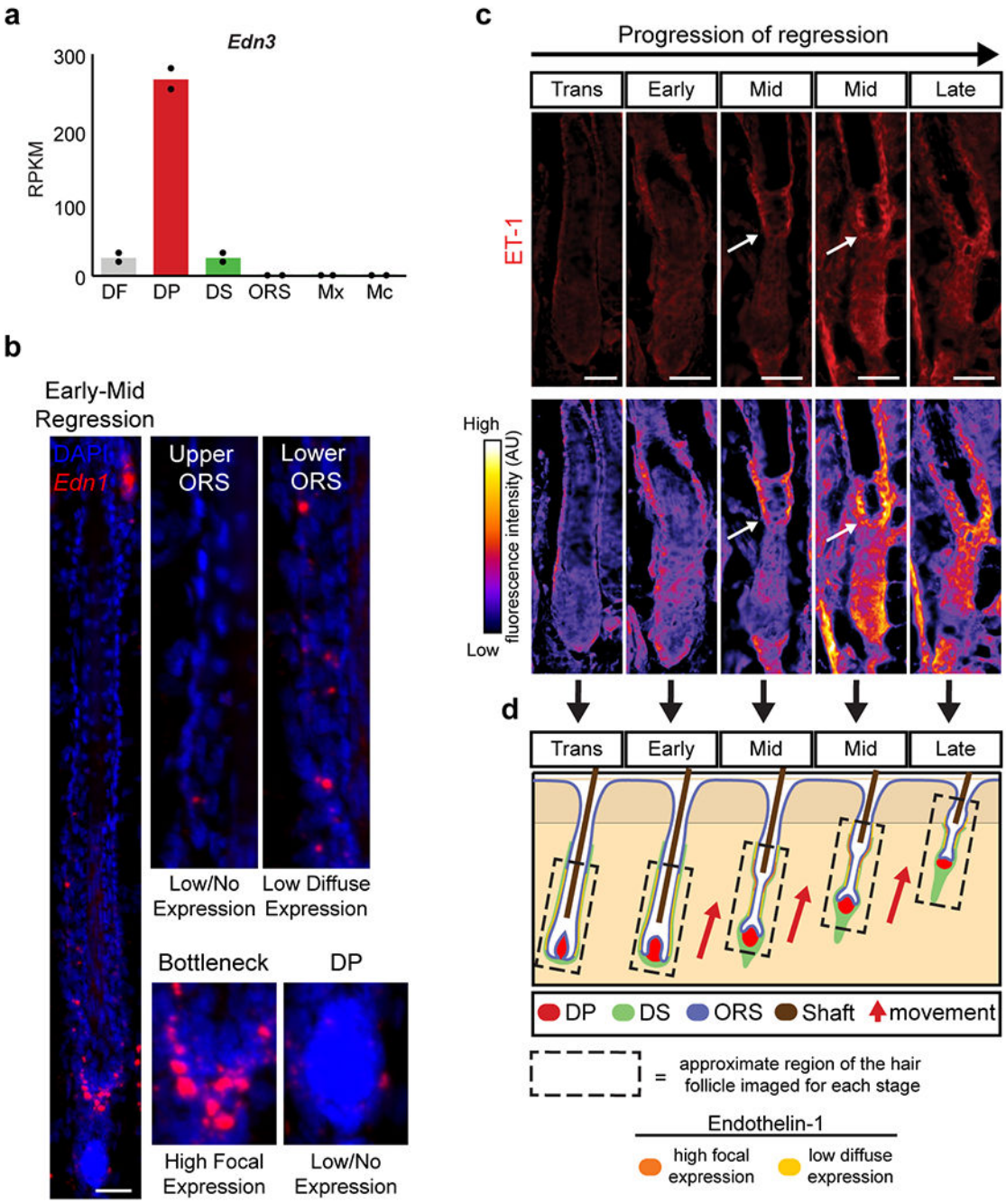

Extended Data Fig. 8. Patterns of endothelin ligand expression during regression

a, *Edn3* mRNA expression across cell types from previously published transcriptome data at P5[20,32](*n* = 2, data are mean with individual data points). **b**, *Edn1* smFISH in a follicle transitioning from early-to-mid regression (*n* = 3 mice). While only very diffuse expression of *Edn1* is detectable throughout most of the ORS, the progenitors located in the bottleneck region of the follicle exhibited very high focal expression of *Edn1*, corresponding to the site of known DS contraction. Scale bars, 50 μm. **c**, Fire LUT conversion of ET-1 immunofluorescence signal from Fig. 5d highlights the high focal expression of ET-1 in

the bottleneck region of regressing follicles. White arrows indicate the bottleneck region. **d**, Schematic of ET-1 expression during different stages of regression.

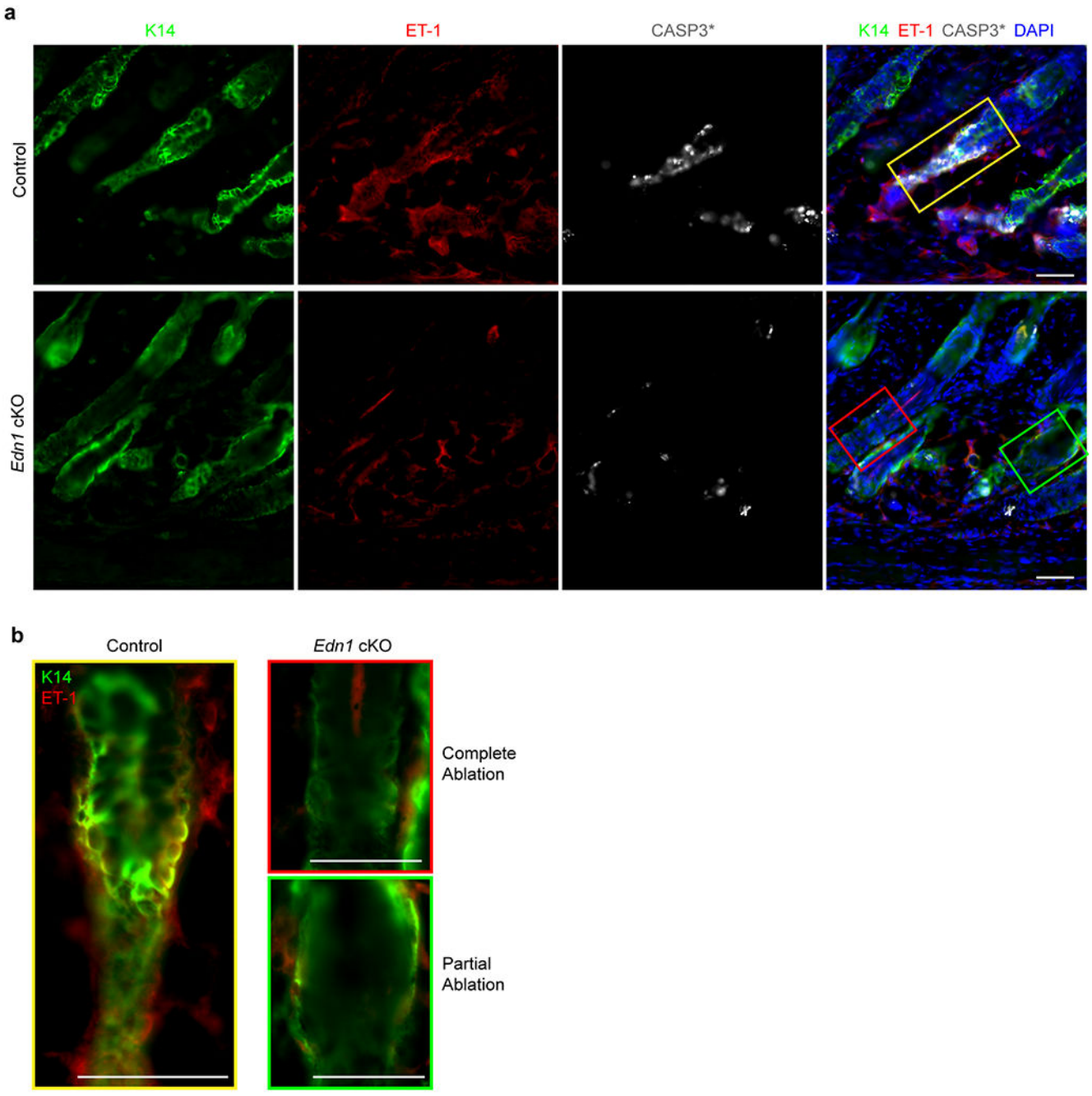

Extended Data Fig. 9. ET-1 ablation in ORS progenitors by mid-regression

Immunofluorescence for K14, ET-1 and CASP3* in P17 back skins from *Edn1* cKO and control ($n = 4$ mice per condition). A marked reduction in both ET-1 and CASP3* in the $K14^+$ ORS progenitors of the HFs in cKO back skins was observed compared to control back skins. Scale bars, 50 μm. **b**, Insets showing K14 and ET-1 colocalization in regressing

HF from control back skin, with high focal expression of ET-1 in the bottleneck region. In *Edn1* cKO back skins, some HFs exhibit complete ET-1 ablation while other HFs only exhibit partial ET-1 ablation in the $K14^+$ ORS progenitors. Scale bars, 50 μm.

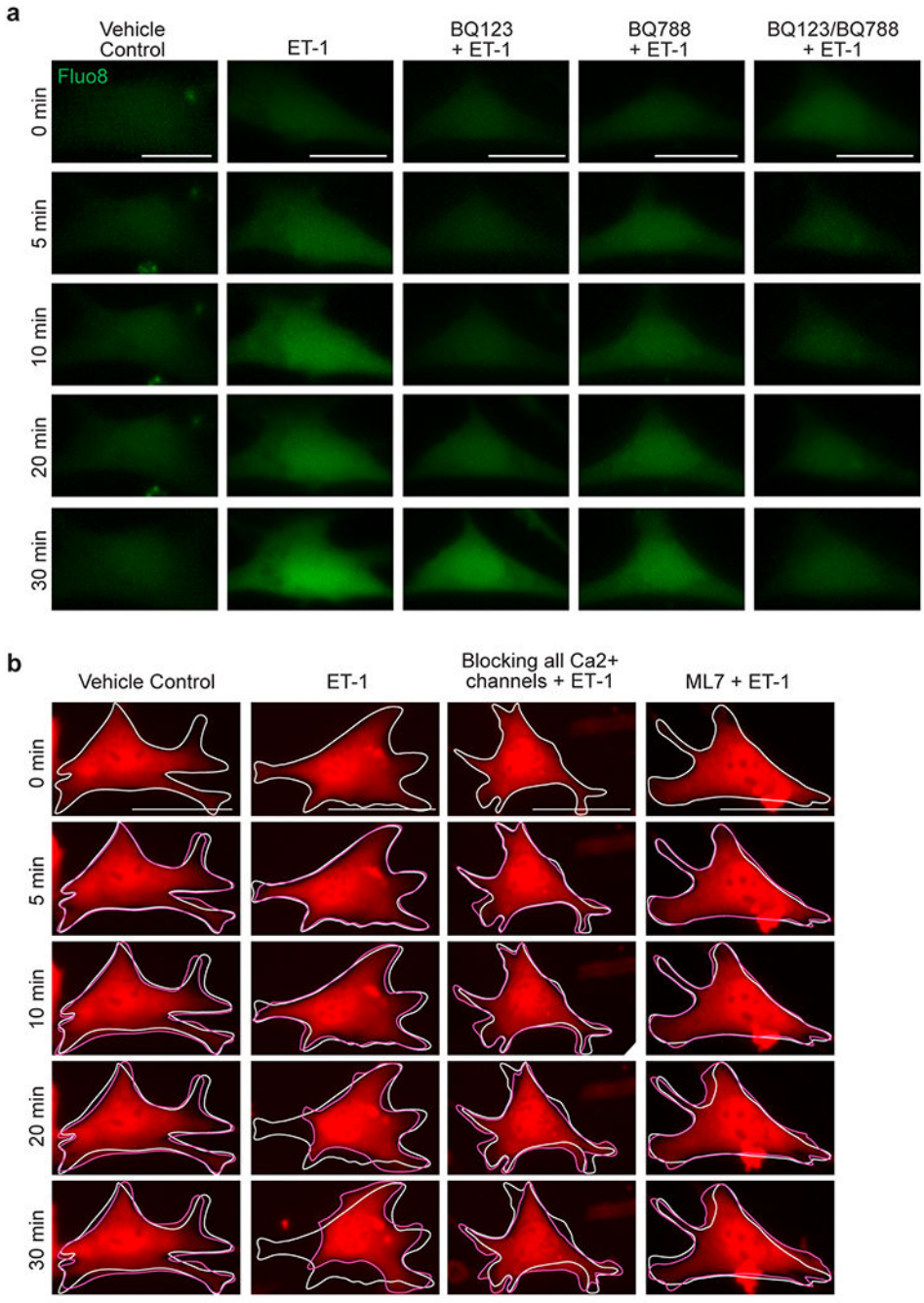

Extended Data Fig. 10. ET-1-induced DS contraction depends on dynamically regulated cytoplasmic Ca^{2+}

a, Images of Fluo8 levels in DS cells from Fig. 7b including intermediate timepoints (5, 10, 20 mins) during the 30-minute ET-1 or vehicle control (PBS) exposure; $n = 2$ independent experiments. Scale bars, 50 μm. **b**, Images of tdT-labeled DS cells at 0, 5, 10, 20 and

30 minutes of ET-1 or vehicle control (PBS) exposure following a 1 h preincubation in calcium channel blockers (50μM NNC 55-0396 + 50 μM Diltiazem + 10 μM Ryanodine + 10 μM Xestospongin C), ML7 (200 μM), or vehicle control (DMSO); $n = 2$ independent experiments. Endothelin-mediated DS contraction is abrogated by either blocking of calcium channels or by inhibition of MLCK activity. Scale bars, 50 μm.

Supplementary Material

Refer to Web version on PubMed Central for supplementary material.

ACKNOWLEDGMENTS

We thank Sarah Millar for thoughtful discussions and comments on the manuscript. Many thanks to David Pollock and Ilse Daehn for sharing the *Ednra*, *Ednrb* and *Edn1* targeted mouse lines and Elena Ezhkova for the *K14-CreERT2* line. Many thanks to Jill Gregory for support with figure illustrations. Many thanks also to the personnel at ISMMS Flow Cytometry, Microscopy, Genomics, and Mouse Genetics CoREs for technical assistance. The ISMMS Microscopy CoRE was supported by NIH Shared Instrumentation Grant IS10RR026639. N.H. was supported by training grant T32GM007280 from NIH/NIGMS, by T32HHD075735 from NIH/NIDCR and F30AR070639 from NIH/NIAMS. N.S. was supported by a fellowship of the Training Program in Stem Cell Research from the New York State Department of Health (NYSTEM-C32561GG). M.Y. was supported by the World Premier International Research Center Initiative (MEXT), JSPS KAKENHI (17H06095, 22H04918) and AMED (JP21zf0127005). M.R. was supported by grants from NIH/NIAMS (R01AR071047, R01AR073259, R01AR077593, R01AR079475) and New York State Department of Health (NYSTEM-C32561GG).

DATA AVAILABILITY

Raw and analyzed RNA sequencing data that support the findings of this study are available in the Gene Expression Omnibus (GEO) repository under accession code GSE215133. Previously published RNA seq data that were re-analyzed here are available under accession code GSE77197 and GSE136996. Source data are provided with this study. All other data supporting the findings of this study are available from the corresponding author on reasonable request.

REFERENCES

1. Jones DL & Wagers AJ No place like home: anatomy and function of the stem cell niche. Nat Rev Mol Cell Biol 9, 11–21 (2008). [PubMed: 18097443]
2. Gonzales KAU & Fuchs E Skin and Its Regenerative Powers: An Alliance between Stem Cells and Their Niche. Dev Cell 43, 387–401 (2017). [PubMed: 29161590]
3. Fuchs E & Blau HM Tissue Stem Cells: Architects of Their Niches. Cell Stem Cell 27, 532–556 (2020). [PubMed: 33007238]
4. Sennett R & Rendl M Mesenchymal-epithelial interactions during hair follicle morphogenesis and cycling. Semin Cell Dev Biol (2012).
5. Rezza A, Sennett R & Rendl M Adult stem cell niches: cellular and molecular components. Curr Top Dev Biol 107, 333–372 (2014). [PubMed: 24439812]
6. Kretzschmar K & Clevers H Wnt/beta-catenin signaling in adult mammalian epithelial stem cells. Dev Biol 428, 273–282 (2017). [PubMed: 28526587]
7. Chacon-Martinez CA, Koester J & Wickstrom SA Signaling in the stem cell niche: regulating cell fate, function and plasticity. Development 145 (2018).
8. Vining KH & Mooney DJ Mechanical forces direct stem cell behaviour in development and regeneration. Nat Rev Mol Cell Biol 18, 728–742 (2017). [PubMed: 29115301]
9. Pathak MM et al. Stretch-activated ion channel Piezo1 directs lineage choice in human neural stem cells. Proc Natl Acad Sci U S A 111, 16148–16153 (2014). [PubMed: 25349416]

10. Aragona M et al. Mechanisms of stretch-mediated skin expansion at single-cell resolution. Nature 584, 268–273 (2020). [PubMed: 32728211]
11. Scadden DT The stem-cell niche as an entity of action. Nature 441, 1075–1079 (2006). [PubMed: 16810242]
12. Scadden DT Nice neighborhood: emerging concepts of the stem cell niche. Cell 157, 41–50 (2014). [PubMed: 24679525]
13. Cotsarelis G, Sun TT & Lavker RM Label-retaining cells reside in the bulge area of pilosebaceous unit: implications for follicular stem cells, hair cycle, and skin carcinogenesis. Cell 61, 1329–1337 (1990). [PubMed: 2364430]
14. Blanpain C, Lowry WE, Geoghegan A, Polak L & Fuchs E Self-renewal, multipotency, and the existence of two cell populations within an epithelial stem cell niche. Cell 118, 635–648 (2004). [PubMed: 15339667]
15. Morris RJ et al. Capturing and profiling adult hair follicle stem cells. Nature Biotechnology 22, 411–417 (2004).
16. Tumbar T et al. Defining the epithelial stem cell niche in skin. Science 303, 359–363 (2004). [PubMed: 14671312]
17. Morgan BA The dermal papilla: an instructive niche for epithelial stem and progenitor cells in development and regeneration of the hair follicle. Cold Spring Harbor perspectives in medicine 4, a015180 (2014). [PubMed: 24985131]
18. Hsu YC, Pasolli HA & Fuchs E Dynamics between stem cells, niche, and progeny in the hair follicle. Cell 144, 92–105 (2011). [PubMed: 21215372]
19. Zhang YV, Cheong J, Ciapurin N, McDermitt DJ & Tumbar T Distinct self-renewal and differentiation phases in the niche of infrequently dividing hair follicle stem cells. Cell Stem Cell 5, 267–278 (2009). [PubMed: 19664980]
20. Clavel C et al. Sox2 in the dermal papilla niche controls hair growth by fine-tuning BMP signaling in differentiating hair shaft progenitors. Dev Cell 23, 981–994 (2012). [PubMed: 23153495]
21. Harshuk-Shabso S, Dressler H, Niehrs C, Aamar E & Enshell-Seijffers D Fgf and Wnt signaling interaction in the mesenchymal niche regulates the murine hair cycle clock. Nat Commun 11, 5114 (2020). [PubMed: 33037205]
22. Yang H, Adam RC, Ge Y, Hua ZL & Fuchs E Epithelial-Mesenchymal Micro-niches Govern Stem Cell Lineage Choices. Cell 169, 483–496 e413 (2017). [PubMed: 28413068]
23. Mesa KR et al. Niche-induced cell death and epithelial phagocytosis regulate hair follicle stem cell pool. Nature 522, 94–97 (2015). [PubMed: 25849774]
24. Paus R & Foitzik K In search of the “hair cycle clock”: a guided tour. Differentiation 72, 489–511 (2004). [PubMed: 15617561]
25. Rompolas P et al. Live imaging of stem cell and progeny behaviour in physiological hair-follicle regeneration. Nature 487, 496–499 (2012). [PubMed: 22763436]
26. Oshimori N & Fuchs E Paracrine TGF-beta signaling counterbalances BMP-mediated repression in hair follicle stem cell activation. Cell Stem Cell 10, 63–75 (2012). [PubMed: 22226356]
27. Greco V et al. A two-step mechanism for stem cell activation during hair regeneration. Cell Stem Cell 4, 155–169 (2009). [PubMed: 19200804]
28. Rompolas P, Mesa KR & Greco V Spatial organization within a niche as a determinant of stem-cell fate. Nature 502, 513–518 (2013). [PubMed: 24097351]
29. Heitman N et al. Dermal sheath contraction powers stem cell niche relocation during hair cycle regression. Science 367, 161–166 (2020). [PubMed: 31857493]
30. Martino P, Heitman N & Rendl M The dermal sheath: an emerging component of the hair follicle stem cell niche. Exp Dermatol (2020).
31. Hébert J, Rosenquist T, Götz J & Martin G FGF5 as a regulator of the hair growth cycle: evidence from targeted and spontaneous mutations. Cell 78, 1–9 (1994). [PubMed: 7518355]
32. Kuo IY & Ehrlich BE Signaling in muscle contraction. Cold Spring Harb Perspect Biol 7, a006023 (2015). [PubMed: 25646377]
33. Grisanti L et al. Tbx18 targets dermal condensates for labeling, isolation, and gene ablation during embryonic hair follicle formation. J Invest Dermatol 133, 344–353 (2013). [PubMed: 22992803]

34. Rendl M, Lewis L & Fuchs E Molecular dissection of mesenchymal-epithelial interactions in the hair follicle. PLoS Biol 3, e331 (2005). [PubMed: 16162033]
35. Rezza A et al. Signaling Networks among Stem Cell Precursors, Transit-Amplifying Progenitors, and their Niche in Developing Hair Follicles. Cell reports 14, 3001–3018 (2016). [PubMed: 27009580]
36. Sennett R et al. An Integrated Transcriptome Atlas of Embryonic Hair Follicle Progenitors, Their Niche, and the Developing Skin. Dev Cell 34, 577–591 (2015). [PubMed: 26256211]
37. Sumner MJ, Cannon TR, Mundin JW, White DG & Watts IS Endothelin ETA and ETB receptors mediate vascular smooth muscle contraction. Br J Pharmacol 107, 858–860 (1992). [PubMed: 1472978]
38. Guan Z, VanBeusecum JP & Inscho EW Endothelin and the renal microcirculation. Seminars in nephrology 35, 145–155 (2015). [PubMed: 25966346]
39. Nava E & Llorens S The paracrine control of vascular motion. A historical perspective. Pharmacol Res 113, 125–145 (2016). [PubMed: 27530204]
40. Fisher SA Vascular smooth muscle phenotypic diversity and function. Physiological genomics 42A, 169–187 (2010). [PubMed: 20736412]
41. Rahmani W et al. Hair follicle dermal stem cells regenerate the dermal sheath, repopulate the dermal papilla, and modulate hair type. Dev Cell 31, 543–558 (2014). [PubMed: 25465495]
42. Kedzierski RM et al. Cardiomyocyte-specific endothelin A receptor knockout mice have normal cardiac function and an unaltered hypertrophic response to angiotensin II and isoproterenol. Mol Cell Biol 23, 8226–8232 (2003). [PubMed: 14585980]
43. Barton M & Yanagisawa M Endothelin: 30 Years From Discovery to Therapy. Hypertension 74, 1232–1265 (2019). [PubMed: 31679425]
44. Davenport AP et al. Endothelin. Pharmacological reviews 68, 357–418 (2016). [PubMed: 26956245]
45. Bagnall AJ et al. Deletion of endothelial cell endothelin B receptors does not affect blood pressure or sensitivity to salt. Hypertension 48, 286–293 (2006). [PubMed: 16801484]
46. Neylon CB Vascular biology of endothelin signal transduction. Clin Exp Pharmacol Physiol 26, 149–153 (1999). [PubMed: 10065337]
47. Zhang YV, White BS, Shalloway DI & Tumbar T Stem cell dynamics in mouse hair follicles: a story from cell division counting and single cell lineage tracing. Cell Cycle 9, 1504–1510 (2010). [PubMed: 20372093]
48. Shohet RV et al. Mice with cardiomyocyte-specific disruption of the endothelin-1 gene are resistant to hyperthyroid cardiac hypertrophy. Proc Natl Acad Sci U S A 101, 2088–2093 (2004). [PubMed: 14764893]
49. Ghosh D et al. Calcium Channels in Vascular Smooth Muscle. Adv Pharmacol 78, 49–87 (2017). [PubMed: 28212803]
50. Stow LR, Jacobs ME, Wingo CS & Cain BD Endothelin-1 gene regulation. FASEB J 25, 16–28 (2011). [PubMed: 20837776]
51. Maguire JJ & Davenport AP ETA receptor-mediated constrictor responses to endothelin peptides in human blood vessels in vitro. Br J Pharmacol 115, 191–197 (1995). [PubMed: 7647976]
52. Ling L, Maguire JJ & Davenport AP Endothelin-2, the forgotten isoform: emerging role in the cardiovascular system, ovarian development, immunology and cancer. Br J Pharmacol 168, 283–295 (2013). [PubMed: 22118774]
53. Cacioppo JA, Koo Y, Lin PC, Gal A & Ko C Generation and characterization of an endothelin-2 iCre mouse. Genesis 53, 245–256 (2015). [PubMed: 25604013]
54. Li KN et al. Skin vasculature and hair follicle cross-talking associated with stem cell activation and tissue homeostasis. eLife 8 (2019).
55. Ge Y et al. Combined knockout of collecting duct endothelin A and B receptors causes hypertension and sodium retention. American journal of physiology. Renal physiology 295, F1635–1640 (2008). [PubMed: 18784261]
56. Cacioppo JA et al. Granulosa cell endothelin-2 expression is fundamental for ovulatory follicle rupture. Scientific reports 7, 817 (2017). [PubMed: 28400616]

57. Ko C et al. Endothelin-2 in ovarian follicle rupture. Endocrinology 147, 1770–1779 (2006). [PubMed: 16410304]
58. Ishimoto S et al. Role of endothelin receptor signalling in squamous cell carcinoma. International journal of oncology 40, 1011–1019 (2012). [PubMed: 22075705]
59. Grimshaw MJ Endothelins and hypoxia-inducible factor in cancer. Endocr Relat Cancer 14, 233–244 (2007). [PubMed: 17639040]
60. Mai HQ et al. Therapeutic targeting of the endothelin a receptor in human nasopharyngeal carcinoma. Cancer science 97, 1388–1395 (2006). [PubMed: 17032313]
61. Gehart H & Clevers H Tales from the crypt: new insights into intestinal stem cells. Nature reviews. Gastroenterology & hepatology 16, 19–34 (2019). [PubMed: 30429586]
62. Peng T et al. Hedgehog actively maintains adult lung quiescence and regulates repair and regeneration. Nature 526, 578–582 (2015). [PubMed: 26436454]

METHODS-ONLY REFERENCES

63. Henry SP et al. Generation of aggrecan-CreERT2 knockin mice for inducible Cre activity in adult cartilage. Genesis 47, 805–814 (2009). [PubMed: 19830818]
64. Madisen L et al. A robust and high-throughput Cre reporting and characterization system for the whole mouse brain. Nat Neurosci 13, 133–140 (2010). [PubMed: 20023653]
65. Li L & Ginty DD The structure and organization of lanceolate mechanosensory complexes at mouse hair follicles. eLife 3, e01901 (2014). [PubMed: 24569481]
66. Patro R, Duggal G, Love MI, Irizarry RA & Kingsford C Salmon provides fast and bias-aware quantification of transcript expression. Nat Methods 14, 417–419 (2017). [PubMed: 28263959]
67. Love MI, Huber W & Anders S Moderated estimation of fold change and dispersion for RNA-seq data with DESeq2. Genome biology 15, 550 (2014). [PubMed: 25516281]
68. Chen EY et al. Enrichr: interactive and collaborative HTML5 gene list enrichment analysis tool. BMC Bioinformatics 14, 128 (2013). [PubMed: 23586463]

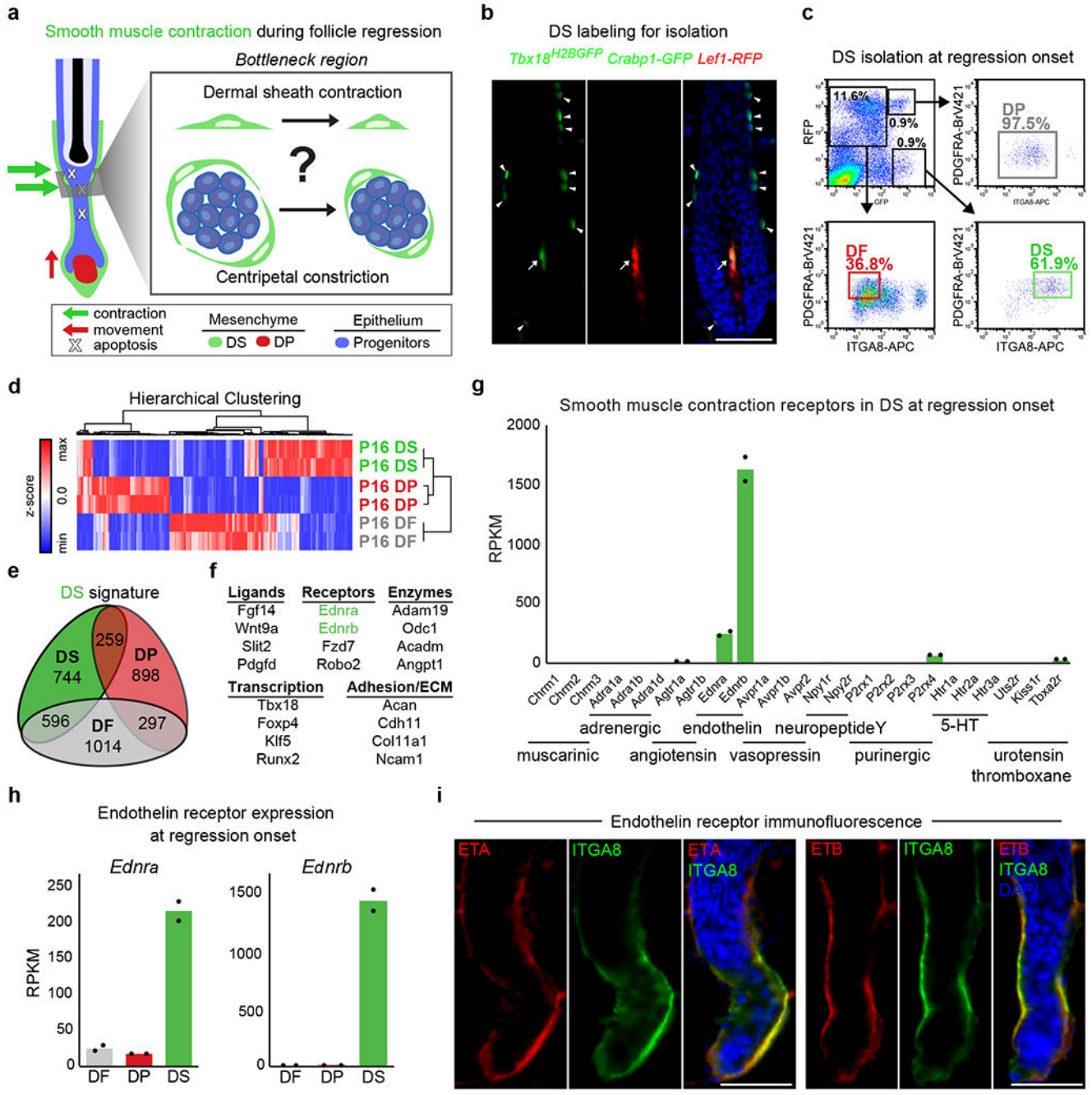

Fig. 1. The dermal sheath expresses receptors of the endothelin signaling smooth muscle contraction pathway.

a, Schematic of regressing hair follicle illustrating apoptosis, contraction and movement processes during the destruction phase of the hair growth cycle. The epithelial progenitor pool (blue) is reduced through apoptosis in the epithelial strand between hair shaft (black) and dermal papilla (DP, red). Dermal sheath (DS) contraction at the bottleneck between epithelial strand and club hair pushes the shaft up and pulls the DP up. As shaft/strand/DP move up towards the stem cell reservoir new progenitors enter the strand

keeping it at a constant length. The molecular mechanisms controlling DS contraction and centripetal constriction are unknown. **b**, Labeling of DS (arrowheads) and DP (arrow) with *Tbx18*^{H2BGFP}*;Crabp1-GFP;Lef1-RFP* transgenic reporters. Scale bar, 50 μm. **c**, Isolation of DS and DP from early-stage regressing follicles (P16) by flow cell sorting of transgenic reporter back skin after immunofluorescence for PDGFRA and ITGA8. DF were isolated for comparison. **d**, Hierarchical clustering of DS, DP, DF with differentially expressed genes. *N* = 2, both replicates are shown. **e**, Venn diagram of gene signatures. **f**, DS signature genes in key gene categories, identifying both endothelin receptors, *Ednra* and *Ednrb*. **g**, Expression levels of receptors of the major smooth muscle contraction-regulating signaling pathways represented as reads per kilobase per million mapped reads (RPKM). *N* = 2, data are mean with individual data points. **h**, DF, DP and DS expression levels of *Ednra* and *Ednrb* at regression onset. *N* = 2, data are mean with individual data points. **i**, Immunofluorescence for endothelin receptors ET_A and ET_B (*n* = 3 mice). ITGA8 marks the DS in regressing P17 hair follicles. Scale bar, 50 μm.

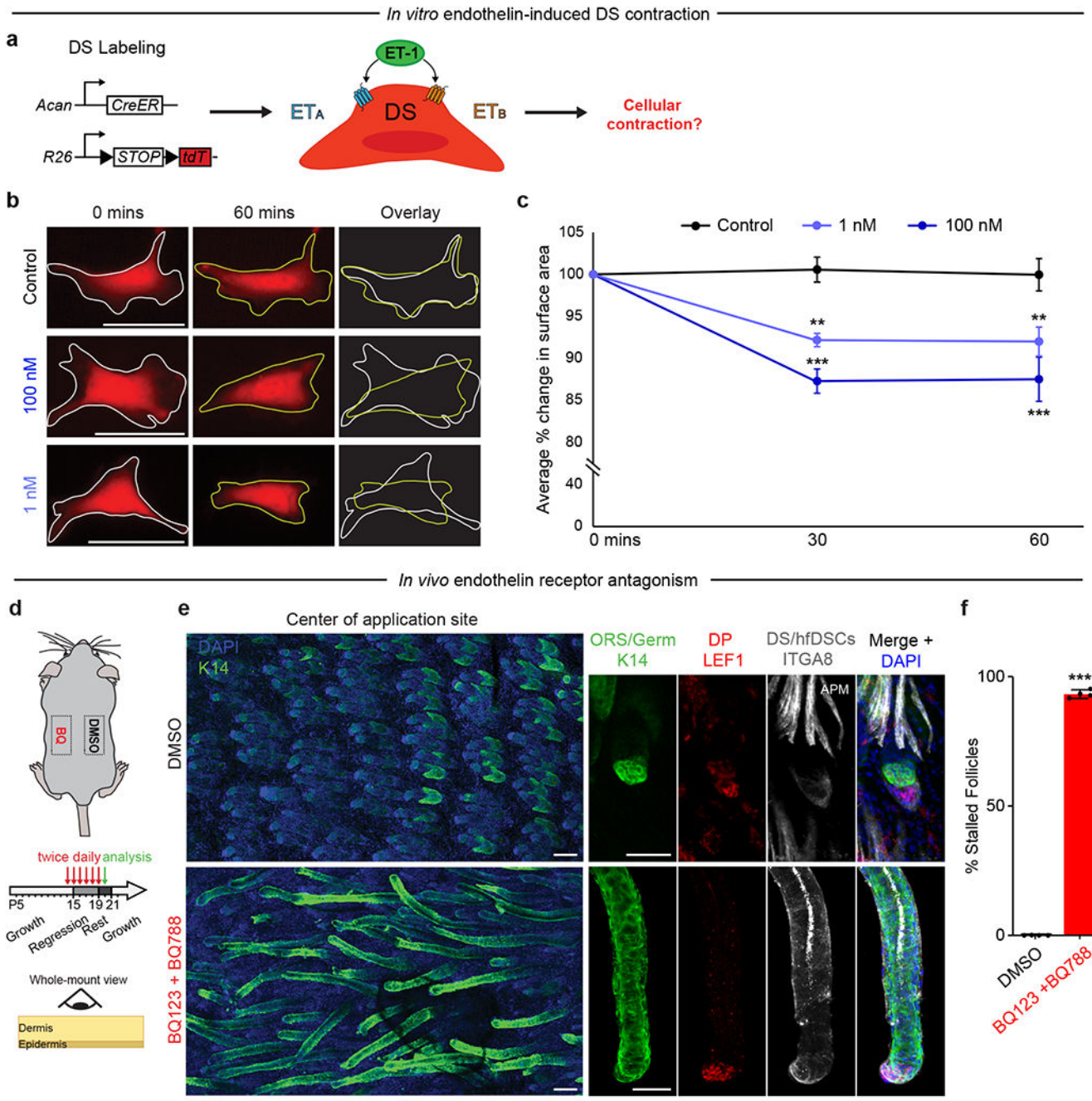

Fig. 2. Endothelin signaling activation contracts DS cells and pharmacological inhibition impairs DS contraction and follicle regression.

a, Schematic of DS contraction *in vitro* assay. Short-term cultured DS cells are genetically labeled with tdTomato (tdT) and incubated with Endothelin-1 (ET-1). **b**, ET-1 triggers DS contraction and surface area reduction in DS cells grown on matrigel. Scale bar, 50 μm. **c**, Quantification of cell surface areas during contraction time course. N = 24, 21, 19 cells for control, 1 nM ET-1, 100 nM ET-1, respectively from three independent experiments. $^{**}P = 0.001$ (30 min) and 0.002 (60 min) for 1 nM ET-1. $^{***}P = 1.24 \times 10^{-5}$ (30 min) and 2.5×10^{-5} (60 min) for 100 nM ET-1. Data are mean ± s.d. and statistical significance

was determined by one-way ANOVA with post-hoc Tukey's HSD for multiple comparison testing. **d**, Schematic of endothelin receptor antagonist BQ123/BQ788 or DMSO topical application to back skin during regression. **e**, Whole-mount immunofluorescence for K14 shows complete regression of follicles into the resting phase of the hair cycle in control-treated back skins, but impaired regression in BQ123/BQ788-treated back skins. Scale bar, 50 μm. **f**, Quantification of the percentage of stalled follicles in the center of the application area (1200 control follicles; 938 BQ123/BQ788-treated follicles; $n = 4$ mice). ***$P = 1.68 \times 10^{-10}$, unpaired two-tailed Student's t-test. Data are mean ± s.d. with individual data points.

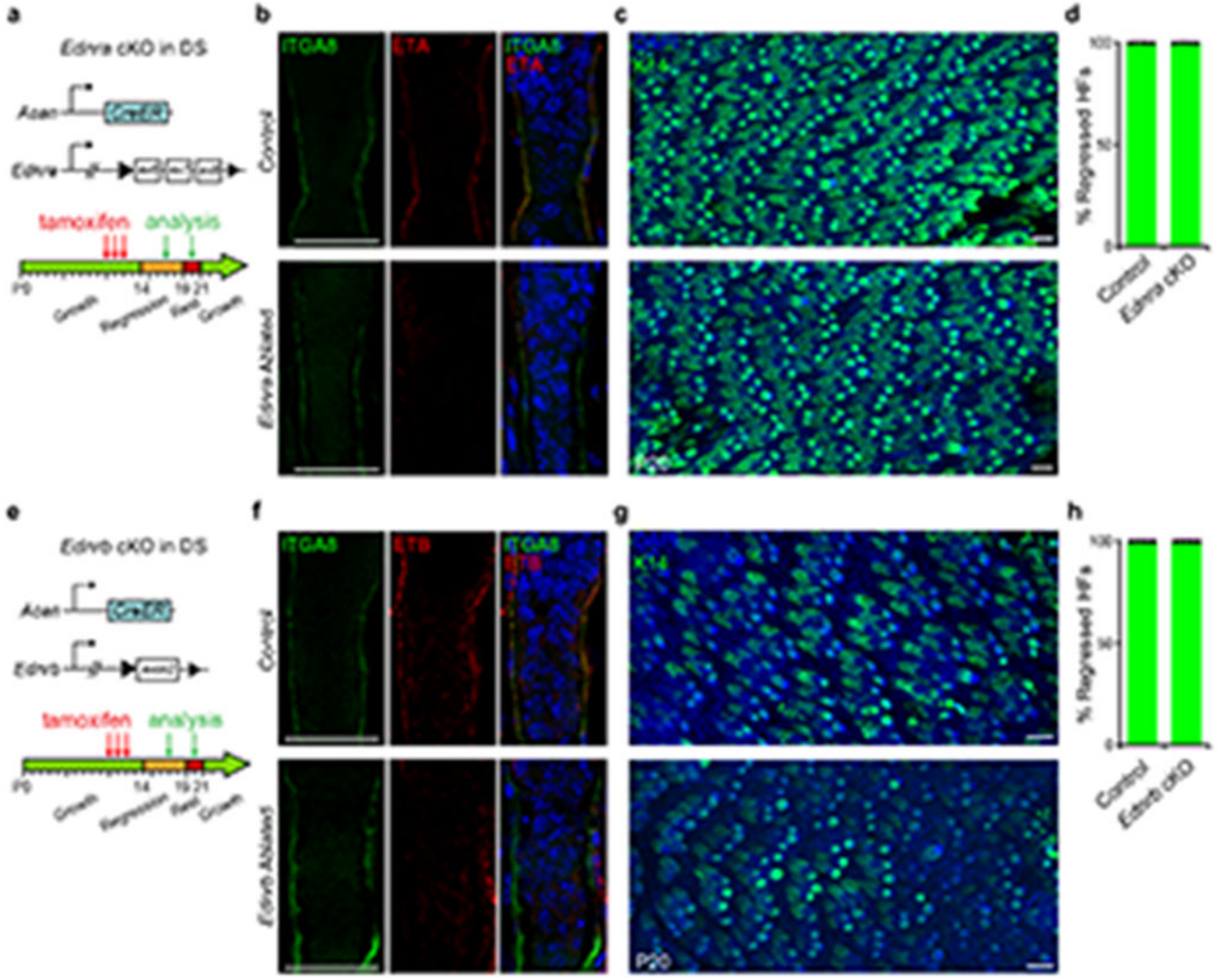

Fig. 3. Genetic ablation of either endothelin receptor does not impair contraction and regression.

a, Schematic of DS-specific *Ednra* conditional knockout (cKO) in the skin. **b**, ET_A ablation by mid-catagen (P17). Immunofluorescence for ET_A imaged in the bottleneck region hair follicles during the regression phase. All follicles in control back skins express ET_A on the surface of $ITGA8^+$ DS. Follicles in *Ednra* ablated back skin lack ET_A in ITGA8-marked DS. Scale bar, 50 μm. **c**, Whole-mount immunofluorescence for K14 shows normal and complete regression of follicles in both control and *Ednra* ablated back skins. Scale bar, 50 μm. **d**, Quantification of fully regressed hair follicles in DS *Ednra* cKO and control back skins (2500 follicles each for control and cKO; $n = 10$ mice). **e**, Schematic of DS-specific *Ednrb* cKO. **f**, ET_B ablation by mid-catagen (P17). Immunofluorescence for ITGA8 and ET_B at the follicle bottleneck. All control follicles express ET_B in $ITGA8^+$ DS. Follicles in *Ednrb* ablated back skin lack ET_B in $ITGA8^+$ DS. Scale bar, 50 μm. **g**, Whole-mount immunofluorescence for K14 shows complete regression of follicles in *Ednrb* ablated back skins. Scale bar, 50μm. **h**, Quantification of fully regressed hair follicles in DS *Ednrb* cKO and control back skins (~2500 follicles each for control and cKO; $n = 10$ mice).

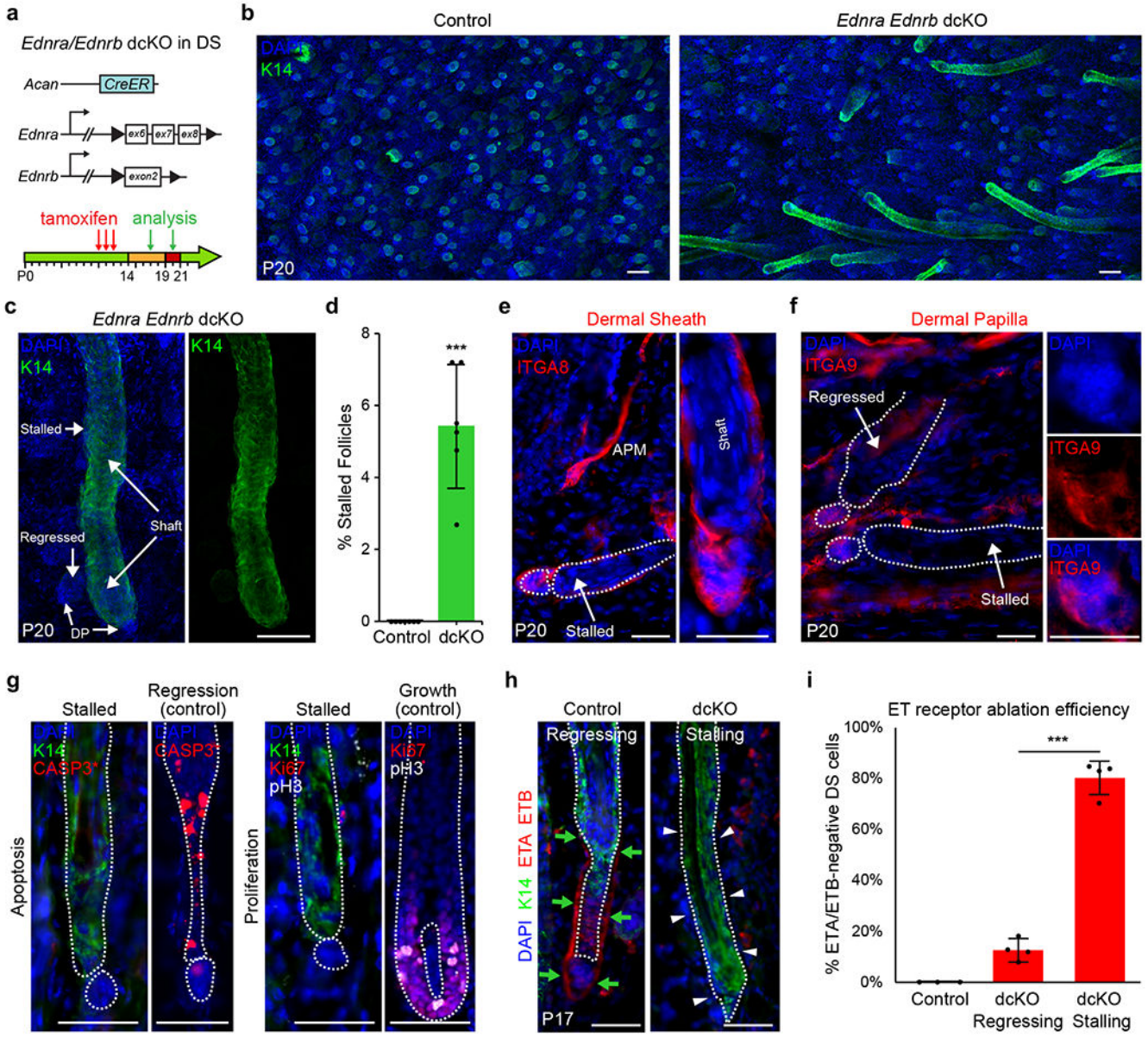

Fig. 4. Genetic dual ablation of both endothelin receptors in the DS impairs follicle regression.

a, Schematic of DS-specific *Ednra* and *Ednrb* double conditional knockout (dcKO). **b**, Whole-mount immunofluorescence for K14 with complete follicle regression in control back skins. In dcKO back skins many HFs failed to regress. **c**, Stalled HFs retained their hair shafts down to the follicle base with DP positioned at the proximal end. Scale bars, 50 μm. **d**, Quantification of stalled follicles in dcKO back skins (3,592 control and 3,731 dcKO follicles; $n = 12$ mice). ***$P = 0.00035$, unpaired two-tailed Student's t-test. Data are mean ± s.d. with individual data points. **e**, Immunofluorescence for ITGA8 of *Ednra;Ednrb* dcKO back skins at P20 ($n = 2$ mice). APM, arrector pili muscle. Scale bars, 50 μm. **f**, Immunofluorescence for ITGA9 in dcKO back skin ($n = 2$ mice). Scale bars, 50 μm. **g**, Immunofluorescence for K14 and apoptosis marker CASP3* or proliferation markers Ki67

and pH3 in dcKO back skin ($n = 2$ mice). $K14^+$ epithelial cells of stalled follicles lack apoptosis and proliferation. Regressing (P17) and growth-phase (P12) follicles served as positive controls. Scale bars, 50 μm. **h**, Immunofluorescence for K14 and ET_A/ET_B in dcKO back skin at P17 demonstrates correlation of stalling phenotype penetrance with ablation efficiency. Only stalled follicles lack both ET_A and ET_B ($n = 4$ mice). Green arrows and white arrowheads highlight the presence and absence, respectively, of ET_A/ET_B in the DS. Scale bars, 50 μm. **i**, Quantification of ET_A and ET_B ablation efficiency in regressing and stalling follicles (30 control follicles, $n = 3$ mice; 39 dcKO regressing follicles and 20 dcKO stalling follicles, $n = 4$ mice). ***$P = 0.00028$, unpaired two-tailed Student's t-test. Data are mean ± s.d. with individual data points.

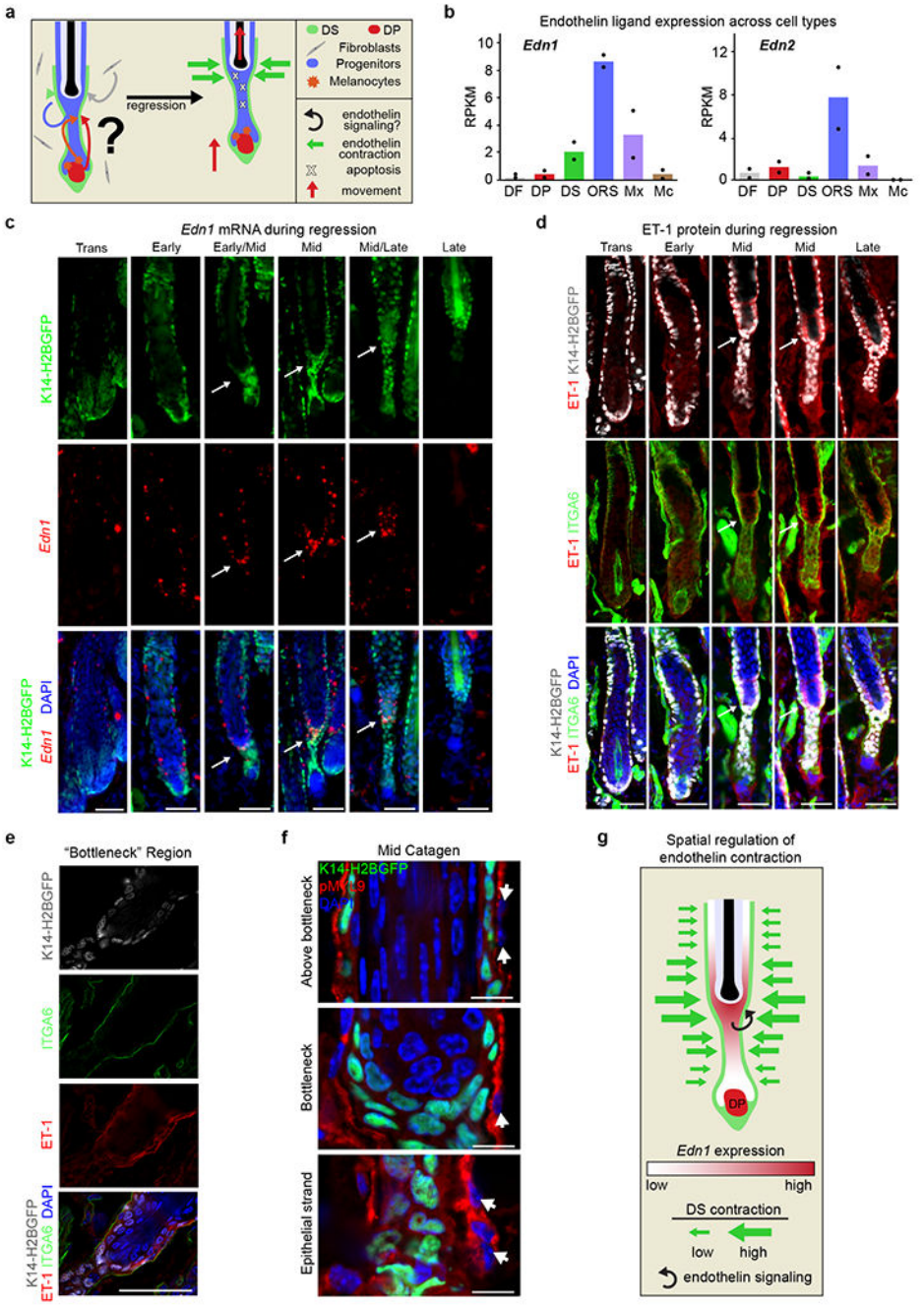

Fig. 5. Spatiotemporal endothelin expression and DS contraction during follicle regression.

a, Schematic illustrating potential sources of endothelin ligand(s) that may induce endothelin receptor activation and DS contraction during regression. **b**, RPKM expression levels of endothelin ligands *Edn1* and *Edn2* from P5 transcriptome data and combined analysis[29,35]. The ORS progenitor population has enriched *Edn1* expression. N=2, data are mean with individual data points. **c**, Single-molecule fluorescence *in situ* hybridization for *Edn1* mRNA during follicle regression phase. Focal expression of *Edn1* is detectable in the bottleneck – corresponding to the known site of DS contraction (n = 3 mice). White

arrows indicate the bottleneck region of the regressing follicles. **d**, Immunofluorescence for ET-1 protein in $K14^{H2BGFP}$ P17 back skins during all stages of the regression phase of the hair cycle, starting from the transition from growth through early, mid and late regression. H2BGFP marks all epithelial cells. ITGA6 marks basal epithelial cells during all regression stages. (n = 3 mice). Low ET-1 expression is seen during the transition ("trans") and early regression. Focal, strong ET-1 upregulation in the bottleneck of mid-regressing follicles. ET-1 expression decreases in the latest stage when the follicle is largely regressed just prior to the rest phase. Scale bars, 50 μm. **e**, High magnification of ET-1 and ITGA6 localization in the bottleneck region of P17 regressing follicle (n = 3 mice). Scale bar, 50 μm. **f**, phospho-Myl9 (activated) immunofluorescence shows enrichment in the DS surrounding and below the bottleneck relative to DS above the bottleneck (n = 2 mice). **g**, Schematic representation of spatially regulated DS contraction by progenitor-derived endothelin.

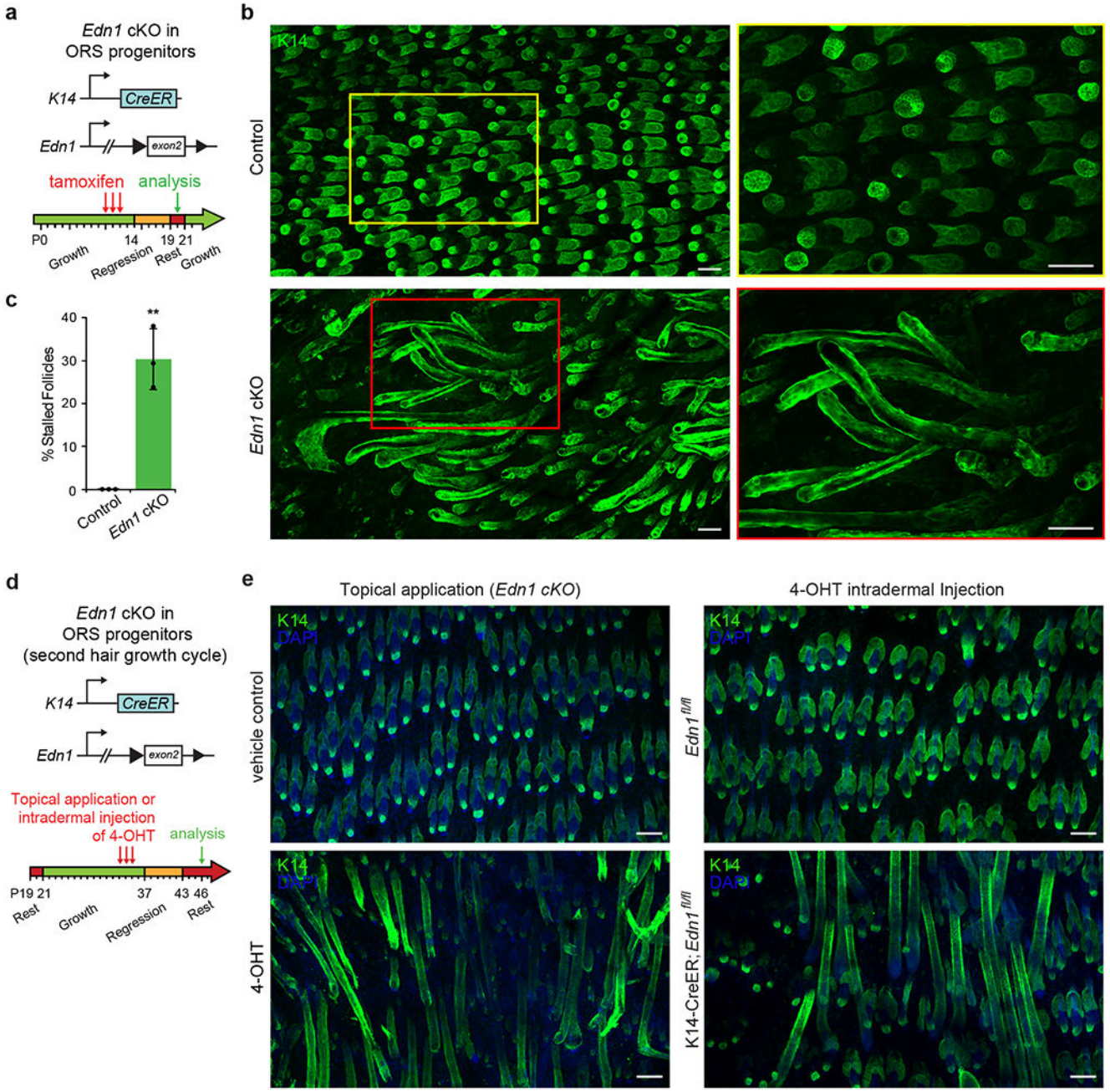

Fig. 6. Endothelin-1 from ORS progenitors is required for follicle regression.

a, Schematic of epithelial-specific *Edn1* cKO during the first hair cycle. **b**, Whole-mount immunofluorescence for K14 reveals massive stalling and failed follicle regression in *Edn1* cKO back skins by P20. Scale bar, 50 μm**. c**, Quantification of stalled follicles in cKO back skins (1500 follicles in control and 1340 in dcKO, $n = 6$ mice). $^{**}P = 0.0018$, unpaired two-tailed Student's *t*-test. Data are mean ± s.d. with individual data points. **d**, Schematic of epithelial-specific *Edn1* cKO during the second hair growth cycle through administration of 4-hydroxy tamoxifen (4-OHT) either by topical application or intradermal injection. **e**, Whole-mount immunofluorescence for K14. Widespread stalling and failed

follicle regression in 4-OHT-induced *Edn1* cKO back skins during the second hair growth cycle (n = 2 mice). Scale bars, 100 μm.

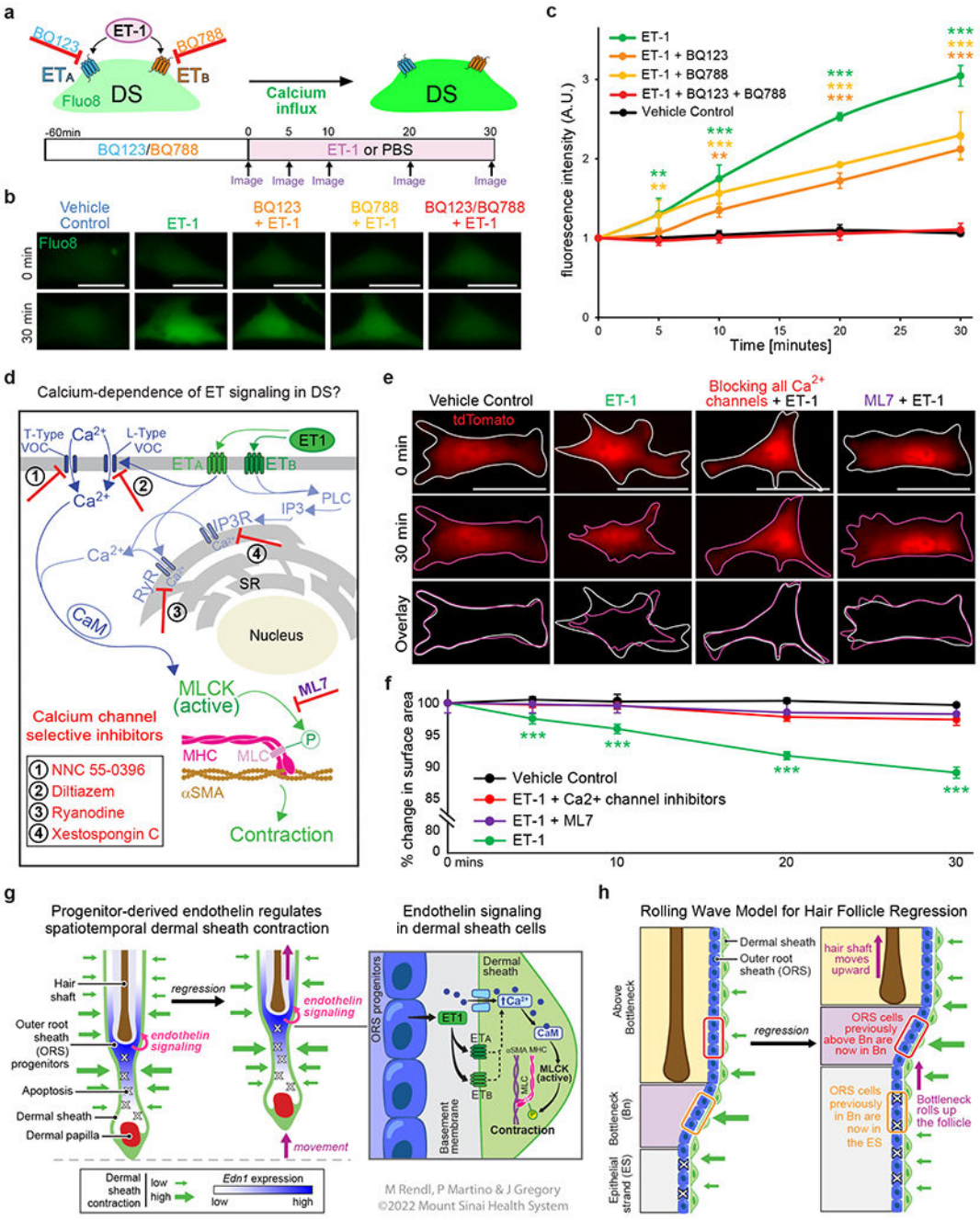

Fig. 7. ET-1 regulates DS contraction through cytoplasmic Ca^{2+} signaling.

a, Schematic of Fluo8 calcium indicator assay to detect cytoplasmic Ca^{2+} in short-term cultured DS cells with ET-1 (1 μM) or vehicle control and preincubations of endothelin receptor antagonists BQ123 (1 μM) and BQ788 (1 μM). **b**, Fluo8 fluorescence in DS cells at 0 and 30 min of ET-1 or vehicle (PBS) with or without preincubation in BQ123, BQ788 or both. Fluo8 levels increased with ET-1, which was partially or fully blocked by individual or combined antagonists, respectively. Scale bars, 50 μm. **c**, Quantification of Fluo8 fluorescence levels. N = 17, 15, 16, 15, 17 cells for control, ET-1, ET-1+BQ123,

ET-1+BQ788, ET-1+BQ123+BQ788, respectively, from two independent experiments. ** $P < 0.01$, *** $P < 0.001$ (P values are listed in methods), one-way ANOVA with post-hoc Tukey's HSD for multiple comparison testing. Data are mean ± s.d. **d**, Schematic of calcium-dependent ET_A/ET_B signaling pathways and small molecule inhibition of calcium channels. **e**, Fluorescence of tdT-marked DS cells at 0 and 30 min of ET-1 (1μM) or vehicle (PBS) exposure following 1h preincubation in calcium channel blockers, MLCK inhibitor ML7, or DMSO control. Scale bars, 50 μm. **f**, Quantification of DS cell surface area over time. $N = 19, 18, 22, 22$ cells for control, ET-1, ET-1+Ca^{2+} channel inhibitors, ET-1+ML-7, respectively, from two independent experiments. *** $P < 0.001$ (P values are listed in methods), one-way ANOVA with post-hoc Tukey's HSD. Data are mean ± s.d. **g,** Schematic of spatiotemporal contraction regulation and molecular mechanism of endothelin signaling. High ET-1 at the bottleneck between epithelial strand and club hair activates endothelin signaling and contraction in neighboring DS. ET-1 binding to endothelin receptors activates Ca^{2+} influx and Ca^{2+}/calmodulin/MLCK signaling resulting in DS cell contraction. **h**, "Rolling wave" model: As the hair shaft gets pushed upwards, the bottleneck and epithelial strand structures move up. ORS cells previously located at the bottleneck become situated in the epithelial strand and undergo apoptosis, while cells previously above the bottleneck now join the bottleneck, produce high ET-1 and regulate DS contraction.